Quaternary Science Reviews 103 (2014) 34–50

Contents lists available at ScienceDirect

Quaternary Science Reviews

journal homepage: www.elsevier.com/locate/quascirev

Iceberg ploughmarks illuminated by shallow gas in the central North Sea

Kjetil E. Haavik*, Martin Landrø

Department of Petroleum Engineering and Applied Geophysics, NTNU, 7491 Trondheim, Norway

ARTICLE INFO

Article history:
Received 30 May 2014
Received in revised form
22 August 2014
Accepted 2 September 2014
Available online 26 September 2014

Keywords:
Iceberg ploughmark detection
Shallow gas
Gas trap
Pleistocene
2/4-14 blowout
AVO analysis
Time-lapse seismic

ABSTRACT

Conventional 3D seismic data provides direct evidence for glacial influence during the early Pleistocene sedimentation in the Central North Sea. We identify iceberg ploughmarks as dim linear to curve-linear features in three early Pleistocene horizons that have high reflection amplitude compared to adjacent horizons. The anomalous horizons are interpreted to be reflections from thin sandy layers saturated with gas. The gas acts as a contrast liquid illuminating the thin sand layers. The reason for this is the difference in acoustic properties between water and gas saturated sand layers. The combination of thin bed effects and shallow gas makes the iceberg ploughmarks easily detectable as dim features in seismic reflection amplitude maps. Our interpretation is based on analysis of real seismic data, well logs and modeled seismic response. The methods we use include interpretation of horizons followed by extraction of reflection amplitudes, well log analysis, pre-stack amplitude versus offset analysis of high resolution 2D seismic data and time-lapse analysis of seismic. Seismic modeling is performed to study interactions between thin sand beds, shallow gas and iceberg ploughmarks. A new trapping mechanism for shallow gas is presented and seismic modeling of this trap strengthens our interpretation. The trap is created by iceberg ploughmarks in sandy layers that are covered by finer and less permeable sediments. For this area we find that conventional seismic interpretation is superior to the much used method of studying seismic time-slices for detection of iceberg ploughmarks, both with respect to time and detectability. This study shows that the interpreter should look for high amplitude horizons with amplitude variations laterally when trying to detect iceberg ploughmarks.

1. Introduction

Icebergs are created by calving ice sheets or glaciers at their marine or lacustrine margins. Interaction between icebergs and the seafloor may result in linear to curve-linear depressions referred to as iceberg scours or iceberg ploughmarks (Woodworth-Lynas et al., 1991). This process can be seen at the present day East Greenland continental shelf (Syvetski et al., 1992; Dowdeswell et al., 1993). Buried Iceberg ploughmarks in the North Sea were first reported by Stoker and Long (1984) and later by others (e.g. Graham et al., 2007; Kuhlmann and Wong, 2008; Dowdeswell and Ottesen, 2013; Haavik and Landrø, 2013). Identifying buried iceberg ploughmarks in seismic data is a much used method to determine whether or not the buried sediments are deposited during a period of glacial influence. Analysis of buried iceberg ploughmarks provides information about the flow direction of the icebergs and potentially their source area. The density of ploughmarks is related to the rate of iceberg production, and should be linked to the dynamics of the ice sheet that produce them (Dowdeswell and Forsberg, 1992). The North Sea Basin has been subsiding throughout the Quaternary, and a close to complete sediment record is preserved in the Central North Sea (Gatliff et al., 1994; Ottesen et al., 2014). These sediments hold key information to map the behavior of the surrounding ice sheets during former glaciations.

Shallow gas has been observed in association with buried iceberg ploughmarks in various ways (Gallagher and Heggland, 1994; Kuhlmann and Wong, 2008; Haavik and Landrø, 2013). Haavik and Landrø (2013) proposed a method for how iceberg ploughmarks act as a trapping mechanism for shallow gas in sand layers. In this paper we describe this trap in more detail and the effect thin gas filled sand layers have on imaging of iceberg ploughmarks. We use seismic data to investigate early Quaternary sediments in the Central North Sea and identify linear to curve-linear features interpreted as buried iceberg ploughmarks in the 2/4 block at approximately 56°4′N and 3°8′E. The interpreted ploughmarks are identified in sediments deposited between the

* Corresponding author.
E-mail address: kjetil.haavik@ntnu.no (K.E. Haavik).

http://dx.doi.org/10.1016/j.quascirev.2014.09.002

Upper Regional Unconformity equivalent (URU) and the Base Naust equivalent as used in Dowdeswell and Ottesen (2013) and Ottesen et al. (2014). We use several geophysical tools such as amplitude vs. offset analysis (AVO), conventional seismic interpretation and time-lapse seismic (4D), together with seismic modeling. The different geophysical tools are explained in Section 3. Here, we use the Quaternary period as formally ratified by the International Commission on Stratigraphy (ISC) that starts at 2.58 Ma and includes the Gelasion stage (Gibbard et al., 2010). We will refer to continuous seismic reflections from geological boundaries as horizons, and we refer to any interface between to different geological layers as a reflector.

2. Background

2.1. Historical setting

The study area is located in the 2/4 block in the Central North Sea (see Fig. 1). In this area shallow gas has been identified as vertical structures and chimneys on seismic reflection data in Paleogene and Neogene sediments over most of the known hydrocarbon reservoirs (D'Heur, 1987; Pekot and Gersab, 1987; Granli et al., 1999). Shallow gas in the Quaternary sediments has been identified within seismic (Lie and Larsen, 1991; Haavik and Landrø, 2013), and also encountered in several exploration wells drilled in this area (according to NPD Fact Pages (2014), wellbore 2/1-1, 2/4-13, 2/4-15 and 2/4-16). A major underground blow out took place when Saga Petroleum drilled the 2/4-14 well into a Jurassic reservoir in 1989. It was estimated that 0.4 MSm^3 of oil and 196-367 MSm^3 of gas had been flowing from the reservoir and into shallow formations before the blow out was killed with assistance from the 2/4-15 relief well after 326 days (Remen, 1991). Lie and Larsen (1991) identified new amplitude anomalies on seismic lines that were re-acquired after the blow out. This was probably the first 4D seismic acquired offshore Norway (Bjørlykke, 2011, Chapter 19). These anomalies were located at approximately 490 m and 840 m below mean sea level and interpreted as the two main recipients for the hydrocarbons from the blow out. The accident has given and will continue to give scientists the opportunity to study the seismic expression of fluid flow in shallow sediments.

The reader is referred to Landrø (2011) for further reading on the 2/4-14 blow out.

2.2. Geological setting

The North Sea was an intracratonic basin during Cenozoic times. With the exception of a narrow seaway that connected the North Sea with the Norwegian-Greenland Sea, landmasses confined the basin: The Fennoscandian shield to the East and Northeast, Central Europe to the South and British Isles to the West (Ziegler, 1988, 1990; Jordt et al., 1995; Sørensen et al., 1997; Huuse et al., 2001; Anell et al., 2011). During most of Paleogene and Neogene, the Central North Sea Basin received sediments from the surrounding landmasses. Continuous subsidence of the basin and uplift of the land areas has governed the evolution of the Central North Sea. An almost complete Cenozoic sediment record is preserved in the central parts of the basin (Ziegler, 1990; Anell et al., 2011). The most accepted model for sedimentation is that the Central North Sea was filled by pro-deltaic and deltaic sediments sourced from North in Oligocene times, gradually rotating clockwise, to supply from Northeast and East in the late Miocene and Pliocene and from East and Southeast in early Pleistocene times (Spjeldnes, 1975; Cameron et al., 1993; Jordt et al., 1995; Sørensen and Michelsen, 1995; Sørensen et al., 1997; Anell et al., 2011; Ottesen et al., 2014). Anell et al. (2011) pointed out that this model was to simple and that sediments were also supplied from the Shetland Platform and Fennoscandia at varying rates throughout this period.

In early Quaternary, the great European rivers provided sediments that filled in the basin from South and Southeast (Bijlsma, 1981; Gibbard, 1988) at the same time as fluvial sediments from the UK area filled the basin from the West (Ottesen et al., 2014). Sediments were also supplied from Denmark from East (Sørensen et al., 1997). The early Quaternary sediments in the North Sea are mainly fluvio-deltaic to marine (Cameron et al., 1987; Long et al., 1988). During the middle and late Quaternary, glacial input to the North Sea was provided by the Scandinavian and British ice sheets that characterized the sediment sources in this period (Stoker et al., 2005). The mid to late Quaternary sediments are related to many cycles of glacial and interglacial periods resulting in inter-bedding of glaciogenic and marine deposits (Jansen and Sjøholm, 1991).

The sediments and erosional features produced in the North Sea basin during the middle to late Quaternary glacial cycles has been studied by many scientists (e.g. Long et al., 1988; Rise et al., 2004; Graham et al., 2010; Stewart and Lonergan, 2011). The North Sea has been inundated by ice sheets several times the last 0.5 Ma, and many generations of buried tunnel valley systems have been mapped in the North Sea (e.g. Cameron et al., 1987; Huuse et al., 2001; Praeg, 2003; Stewart and Lonergan, 2011). Tunnel valleys are erosional features that are formed below ice sheets (Ó Cofaigh, 1996). Several reconstructions of North Sea ice sheet from the late Pleistocene has been proposed (e.g. Ehlers, 1990; Graham et al., 2011; Clark et al., 2012). Less material is published on the early Pleistocene glaciations in the North Sea (Ehlers and Gibbard, 2008). In the Central North Sea, ice-rafted debris (IRD) have been identified in cuttings and cores from the early Quaternary sediments (Eidvin et al., 1999), and iceberg ploughmarks are interpreted in

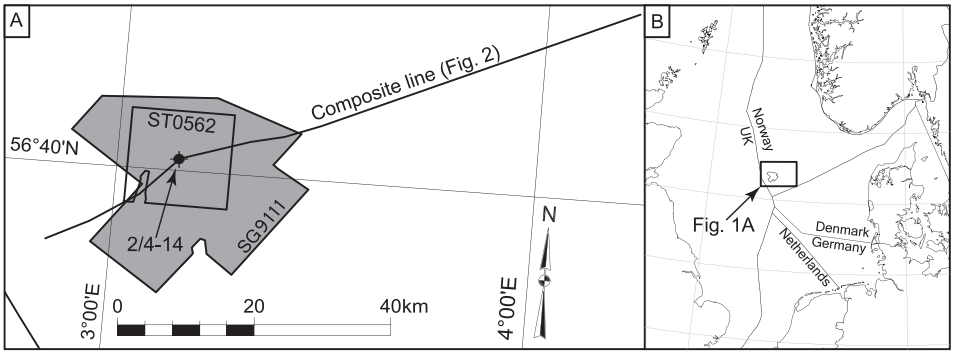

Fig. 1. (A) A map of the study area in the Central North Sea showing the position of the data used in this paper. The position of the 2/4-14 well is indicated together with the position of a composite seismic section and the outline of two 3D seismic cubes, SG9111 from 1991 and ST0562 from 2005. (B) Location map. Our study area is highlighted with a black box.

seismic data continuously through early Quaternary sediments (Dowdeswell and Ottesen, 2013) providing strong, but indirect evidence for glacial influence during this period (Ottesen et al., 2014). The buried iceberg ploughmarks observed in the early Pleistocene sediments in the Central Norths Sea show a principal flow direction in a North-South direction and source of these icebergs was probably a Scandinavian ice sheet (Dowdeswell and Ottesen, 2013). Based on comparison between the dimensions of the early Quaternary iceberg ploughmarks in the Central North Sea with the iceberg ploughmarks observed from modern polar continental shelves, Dowdeswell and Ottesen (2013) conclude that the ploughmarks observed in the Central North Sea are formed in relatively deep water.

2.3. Shallow gas

Gas present in sediments down to 1000 m is referred to as shallow gas (Davis, 1992). Shallow gas in sedimentary basins can have biogenic and/or thermogenic origin. Thermogenic gas is the term used for gas that is generated when organic matter is degraded under high temperature and pressure, and biogenic gas is the term used for microbial degradation of organic matter resulting in gas. Determining the origin of the gas can be done through isotope analysis of gas samples (Floodgate and Judd, 1992) There are several motivating factors for identifying shallow gas: (1) Shallow gas can be used in hydrocarbon exploration as an indicator that there is a working petroleum system present (e.g. Heggland, 1998). (2) Shallow gas is a potential geohazard for drilling operations. Gas may be present in pressurized pockets, trapped beneath low permeability shale and form a blow out hazard (Sillis and Wheeler, 1992). (3) Shallow gas may be produced (Peon discovery in the Norwegian Sea). (4) Shallow gas reduces the seismic velocity of the sediments significantly. Including knowledge of shallow gas when making velocity models will improve seismic imaging (Sernpere and Hardy, 1998).

The use of conventional 3D seismic data has proven valuable for identifying shallow gas (Gallagher and Heggland, 1994; Sallisbury et al., 1996). Shallow gas has many expressions in seismic data and descriptions of these can be found in e.g. Judd and Hovland (1992) and Løseth et al. (2009). Two of most obvious gas effects that can be seen in seismic data are bright spots due to gas accumulation, and chimneys due to dispersed gas that reduce the velocity of the affected sediments and obscure the image (e.g. Arntsen et al., 2007).

3. Database and methods

3.1. Data

The data sets available for this study are two industry 3D seismic cubes, 2D regional lines and high resolution 2D lines from site surveys. The two 3D data sets SG9111 and ST0562 were acquired in 1991 and 2005, respectively, and the 2005 cube is fully embedded within the 1991 cube. They have been acquired along different sail lines and processed differently. The bin-size in the both the 3D data sets are 12.5 m × 25.0 m and the temporal sampling is 4 ms. The 3D data sets are processed to zero phase wavelet and the central frequency is about 45 Hz in the shallow parts. Interpretation of the 3D seismic data is only available in full-stack migrated versions, which means that no information about angle dependent reflection amplitudes are available (see Section 3.4 on AVO). The quality of the 3D data sets is poor in the shallow parts that are studied here. This is because few or none of the processing steps have been optimized for the shallow parts. The 2D high resolution lines are from the SG8845, SG8910 and ST09322 site/monitor surveys and have a common mid-point (CMP) separation of 6.25 m, an offset range from 41 m to 1200 m and the temporal sampling is 1 ms. The wavelet is processed into a zero-phase wavelet and the central frequency is close 70 Hz. Some of the 2D lines are available in pre-stack format. The regional seismic 2D lines used in this study are CAST-90-122A and UG97-112. They have CMP separation of 12.5 m and the temporal sampling is 4 ms. The wavelet for these lines are mixed phase wavelet and the central frequency is between 25 and 40 Hz. A sparse set of well logs are available from the area. This reason for this is that most of the wells have not been logged in the shallow parts. Gamma ray logs are available in the shallow parts from wells 2/4-10, 2/4-13, 2/4-16 and 2/4-17. A Sonic log is available from the 2/4-16 well. The data set is provided by the sponsors of the LOSEM consortium at NTNU.

3.2. Regional stratigraphy

A representative Southwest-Northeast trending seismic composite line across the Southern part of the North Sea in Norway is shown in Fig. 2. This line is composed of the lines CAST90-122A, a random profile through the SG9111 and the UG97-122 line, indicated in Fig. 2. In this study we have picked four geological horizons on a regional scale. The purpose of this is to set the studied interval in relation to previous work. Three of the horizons are tied to the interpretation in Fig. 4 from Anell et al. (2011). These horizons are BASE NEO 2, BASE NEO 3 and BASE NEO 4, and corresponds to the Mid-Miocene Unconformity (MMU), the Base Naust equivalent and the Upper Regional Unconformity (URU) equivalent that are the names used in this paper, respectively. The Mid Miocene Unconformity corresponds to the base of the Nordland Group after Deegan and Scull (1977) and is a well described regional unconformity in the North Sea (e.g. Jordt et al., 1995; Sørensen et al., 1997; Michelsen, 2001). The Base Naust and the URU are horizon that are well defined in the Norwegian sea (Dalland et al., 1988; Rise et al., 2005; Ottesen et al., 2009) and were extended from the Norwegian sea to the North Sea in Dowdeswell and Ottesen (2013). On the mid-Norwegian Shelf the Naust Formation is mainly of glacial origin and its base is about 2.75 Ma (Rise et al., 2005), older than base of Quaternary. The age of URU is close to the Brunhes-Matuyama magnetic boundary at 0.78 Ma (Stoker et al., 1983) in the Norwegian sea, and its equivalent in the North Sea is probably younger than this (Ottesen et al., 2014). The URU is the boundary between the early and middle Pleistocene. The fourth horizon that was picked is called Gas Level 1, and is the deepest horizon where we identify dim linear to curve-linear features in a high amplitude background as described in Section 3.3.

3.3. Iceberg ploughmark detections

A much used method to detect buried iceberg ploughmarks in seismic data has been through step-wise time slicing through 3D cubes and identifying linear to curve-linear features (e.g. Dowdeswell and Ottesen, 2013). Here, we identify three dipping horizons in the seismic that have anomalous amplitudes and exhibit amplitude variations laterally. These horizons are positioned between 500 ms and 700 ms and have been picked within the 1991 3D seismic data set. A close up of these horizons are shown in Fig. 3. The horizons were picked on zero crossing in a filtered version of the cube, and attributes were extracted from the seismic data along these horizons afterward. The filter that was used was a spatial and temporal smoothing filter. Picking zero crossings proved to be simpler and more robust than picking on peak (maximum positive amplitude) or trough (maximum negative amplitude). The reason for this is probably because of the great lateral amplitude variations that makes it hard for tracking

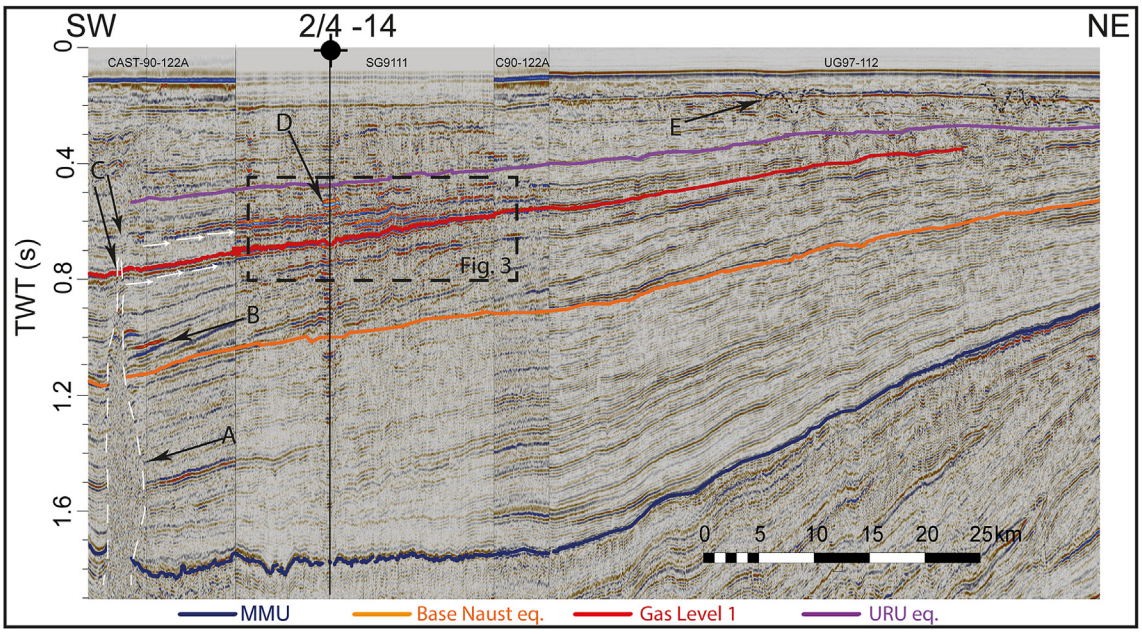

Fig. 2. A composite seismic profile as shown in Fig. 1. Base NEO2, Base NEO3 and Base NEO4 are horizons that are tied to previous work in the North Sea (see Anell et al., 2011, Fig. 4). Gas Level 1 is the deepest of the three horizons which are further studied in this paper (see Section 3.3). The position of the 2/4-14 well bore is indicated. Arrows: (A) A gas chimney that shows that gas from deeper strata has migrated vertically. (B) Bright spots indicate accumulation of gas in porous sediments. (C) Possible entry points for lateral migration for the shallow gas in the sand layers investigated in this work. Possible lateral migrations routes from the gas chimney are indicated by white arrows. (D) The amplitude anomaly at 550 ms is a known gas accumulation with gas from the 2/4-14 underground blow out. (E) Tunnel Valleys in the middle and late quaternary.

algorithms to continue tracking. The horizons corresponding to Gas Level 1 and 3 in Fig. 3 could be traced through the entire data set, while the horizon corresponding to Gas Level 2 is truncated towards Northeast. In this region, careful picking was performed to ensure that the layers that were positioned above or below the original horizon continued to stay above or below the picked horizon. The position of the truncation is indicated with an arrow in Fig. 3 (and a dashed white line in Fig. 6). Root-Mean-Squared (RMS) amplitudes were extracted from the unfiltered seismic cube in an 18 ms window centered on each of the picked reflectors. Different attributes (e.g. variance, coherency) were tested, but we found that the RMS amplitude attribute gave the best result for visualizing these dim linear to curve-linear features.

A two-way travel-time map of the horizon corresponding to Gas Level 1 is shown in Fig. 4. The RMS amplitude attribute maps generated from the three levels in Fig. 3 are shown in Figs. 5–7. Time slices that cut through these features at two different constant travel times are shown for the purpose of comparison with the method used here in Fig. 8, and the position of these are indicated by white dashed boxes in Figs. 5–7. The dim linear to curve-linear features observed in the three gas levels were interpreted one by one and directional analysis was performed by mapping the orientation of each of these. The interpreted dim linear to curve-linear features from all three gas levels are presented in Fig. 9 with corresponding rose diagrams showing the orientation of the features.

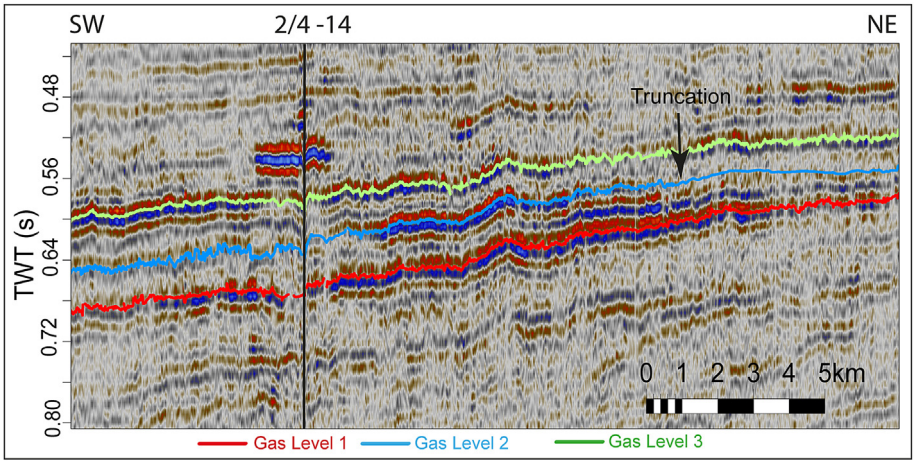

Fig. 3. Shallow seismic profile showing the three anomalous horizons Gas Level 1 (red), Gas Level 2 (blue) and Gas Level 3 (green). These Horizons have been picked through the SG9111 data set. This section is the part of Fig. 2 that runs through the SG9111 3D seismic data shown in Fig. 1. The position where Gas Level 2 truncates is indicated with an arrow.

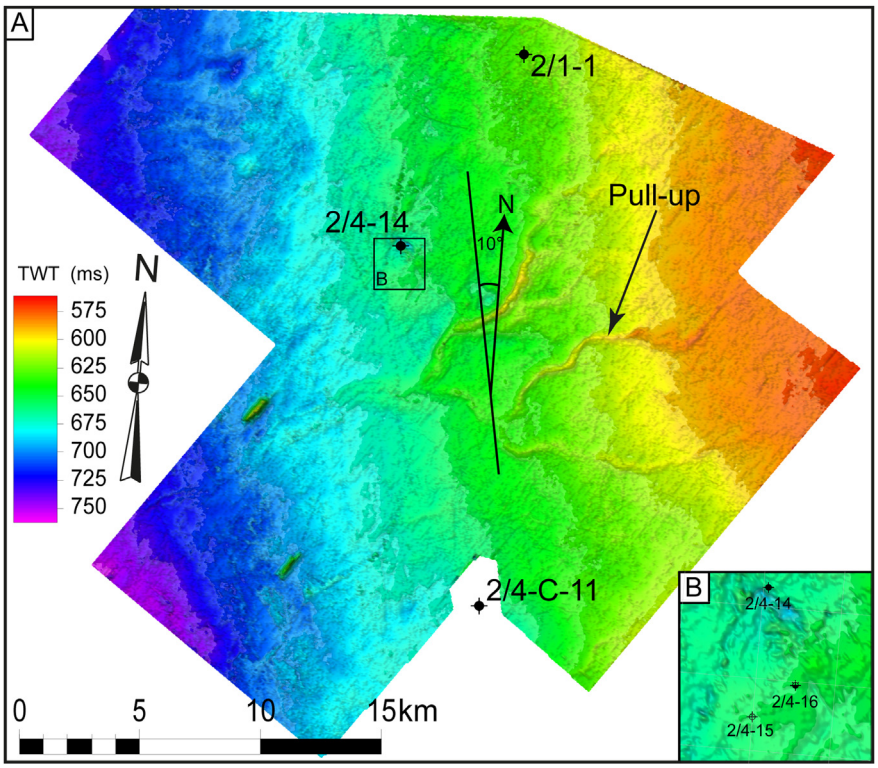

Fig. 4. (A) A Two-way travel time map of the horizon corresponding to Level 1 in Section 3.3. The units are in milliseconds. The layer has an average dip of 0.3° towards Southwest. The strike angle is 10° Northwest. The arrow indicates pull-up that is associated with high velocity infill of tunnel valleys (e.g. Ó Cofaigh, 1996) that are located in Middle to Late Quaternary sediments positioned above. The position of the 2/1-1, 2/4-14 and 2/4-C-11 wells are indicated, and a close up of the wells that are positioned in the vicinity of the 2/4-14 well is shown in (B).

3.4. Amplitude versus offset analysis

Amplitude versus offset (AVO) analysis is a method that can provide information about lithology and fluid content based on angle dependent reflection coefficients (Smith and Gidlow, 1987; Hampson and Russell, 1990). A pre-stack high resolution 2D seismic line from 1988 was used in the AVO analysis. The data was sorted into common mid points (CMP) and the reflector corresponding to Gas Level 2 was picked for analysis. CMPs from two areas that are shown in Box 1 and Box 2 in Fig. 10A were used in the AVO analysis. The position of this 2D line is superimposed on the RMS amplitude map from Section 3.3 shown in Fig. 10C. RMS amplitudes were extracted from a 10 ms window, and corrected for both geometrical spreading and attenuation. Compensation for attenuation loss was done using a constant Q model with peak frequency $f_p = 70\ Hz$, $Q = 70$ and the travel-time was estimated by a simple straight ray-tracing procedure. The same rays were also used when correcting for geometrical spreading. Finally, the amplitudes were multiplied by -1 to change the polarity back to negative, as we would expect from a reflection from the boundary between shale and a poorly consolidated sand that is saturated with gas. This was done because the result of the RMS process is always a positive number. The gamma ray log from the shallow parts of 2/4-16 Well is shown in Fig. 10B. The interval marked in Blue, at approximately 560 m, has been interpreted as a 6 m thick sandy layer. We interpret this as sand because of the low gamma ray count. This layer corresponds to Gas Level 2 in Section 3.3. We observe low gamma ray values around 530 m, 580 and 605 m. The layers at 530 m and 605 m correspond to Gas Level 1 and 3, respectively.

AVO modeling was performed in order to compare the field data to different scenarios of pore fluids. Our hypothesis is that the strength of the amplitudes in the three gas levels are related to the pore fluids. To model AVO responses, a model consisting of two layers was used: A porous sandstone layer below a layer of shale. P-wave velocity (α) was chosen based on well logs. S-wave velocity (β) and density (ρ) are also required for the AVO-modeling, but were not available from logs. To get an estimate of S-wave velocities in both layers we used the empirical relationship given by Han (1986), which uses P-wave velocity as input. Velocities for sandstone saturated with both water and methane gas, and mixtures of the two, were found using fluid substitution (Gassman, 1951). Velocities were found for two different types of saturations: gas uniformly distributed in water and for patches of concentrated gas in water background. These types are referred to as uniform and patchy saturation, respectively. The reflection coefficients were calculated using an approximation to the equations in Zöppritz (1919) given in Shuey (1985). A brief summary of how to perform AVO analysis and the equations needed for this process is given in Appendix 1. The parameters used for the water saturated sandstone layer was $\alpha_{sw} = 1900\ m/s$, $\rho_{sw} = 2.07\ g/cm^3$ and porosity $\phi = 0.35$. For the shale layer we used $\alpha_{sh} = 2100\ m/s$, $\rho_{sh} = 2.13\ g/cm^3$. The field data was normalized to the modeled data. This was done by finding a scaling factor that scaled the regression line from the data points from the presumed water filled zone to the amplitudes calculated for the scenario where the sandstone is saturated with 100% water. This scaling factor was then applied to all data points.

The data from the AVO analysis of the pre-stack high resolution 2D data are shown together with modeled AVO response in Fig. 11.

3.5. Time-lapse seismic (4D) analysis

Time-lapse, or repeated seismic is a commonly used tool in the petroleum industry when designing infill production or injection

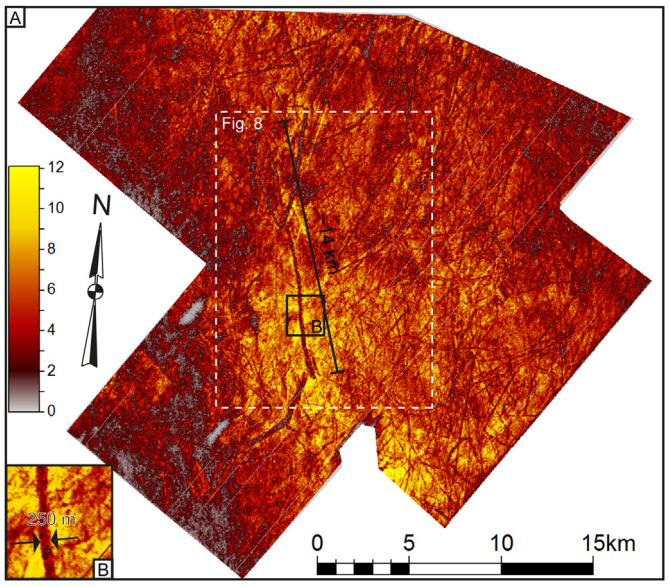

Fig. 5. (A) RMS amplitude map extracted from the unfiltered SG9111 data in an 18 ms window around the horizon corresponding to Level 1 in Section 3.3. The black scale shows the length of the largest continuous dim line that is approximately 14 km long. The width of this dim line is found to be up to 250 m if they are measured between the high amplitudes on both sides. A close up of how and where the width is measured is shown in (B). The area inside the dashed with Fig. 8 box is shown together with a time slice at 680 ms in Fig. 8 A1 and B1, respectively.

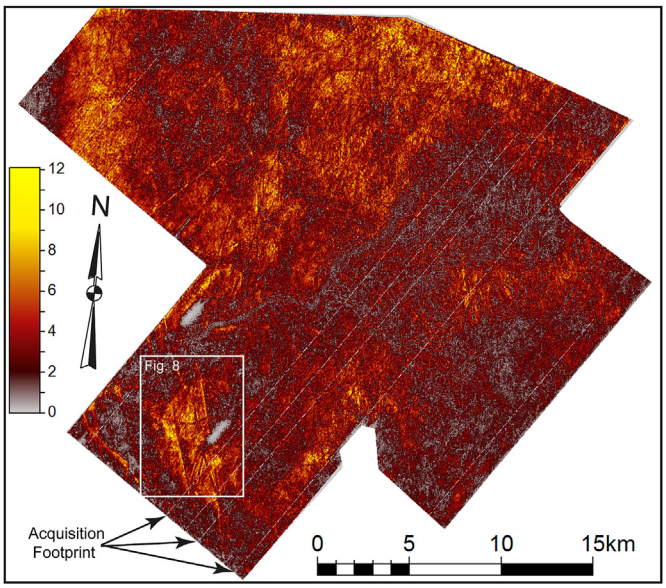

Fig. 7. RMS amplitude map extracted from the unfiltered SG9111 data in an 18 ms window around the horizon corresponding to Level 3 in Section 3.3. Dim lines can be seen in the high amplitude areas. Acquisition footprints are seen as parallel dim lines running in the towing direction. The area inside the dashed with Fig. 8 box is shown together with a time slice at 600 ms in Fig. 8 A3 and B3, respectively.

wells and deciding on injection/production strategy for hydrocarbon reservoirs (Greaves and Fulp, 1987; Landrø et al., 1999). When two seismic data sets are acquired over the same area with a given time period in between, they can provide insight into how geology, fluid content and pressure may have changed over this period (Landrø, 2001). Here we perform time-lapse studies on the two 3D seismic data sets acquired in 1991 and 2005, respectively, and on three 2D high resolution seismic lines that are acquired over the same physical line in 1988, 1990 and in 2009.

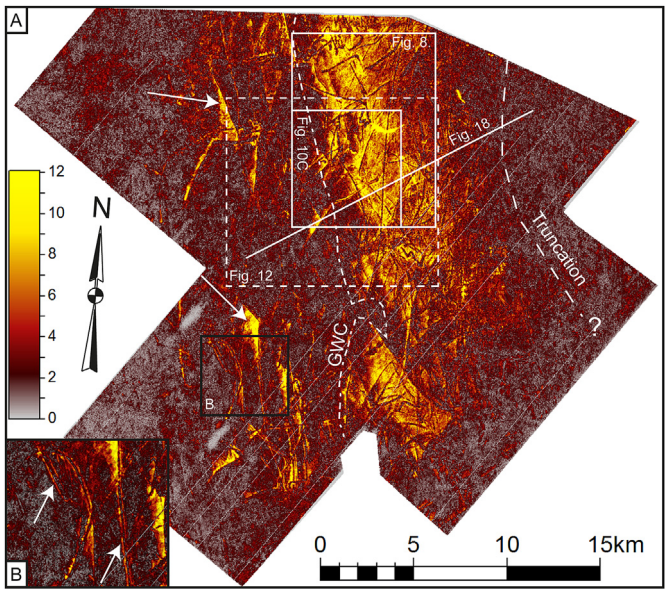

Fig. 6. (A)RMS amplitude map extracted from the unfiltered SG9111 data in an 18 ms window around the horizon corresponding to Level 2 in Section 3.3. The truncation of the reflector corresponding to Gas Level 2 is indicated along. The GWC line is the approximate boundary of the high amplitude belt that is seen in close to North-South trend. The arrows are indicating some of the triangular shaped anomalies that can be observed in this map. Larger figures are available of the indicated boxes. The area inside the dashed with Fig. 8 box is shown together with a time slice at 600 ms in Fig. 8 A2 and B2, respectively. (B) High amplitude curve linear features are indicated with white arrows. These features are seen in pairs. (B) Is a close up of the black box in (A).

The two-way travel-times (TWT) down to a given geological reflector are different in the 1991 and 2005 3D seismic data sets, on a regional scale. This difference is not related to any changes in the geology over this period, but a result of different processing work flows that have been applied to the respective data sets, and most important, the velocity models used for imaging of the two data sets are known to be different. This difference makes it essential to recognize and pick the same geological reflector and perform attribute analysis in both data sets. The horizon corresponding to Gas Level 2 (in Section 3.3) was picked throughout the 2005 3D seismic data set and the same procedure for extracting RMS amplitudes as discussed in Section 3.3 was carried out. Since the two 3D seismic data sets are acquired and processed differently they have different range of amplitudes. This difference in amplitudes is depth dependent and could not be adjusted for globally. However, a local scaling of the 2005 data set at the investigated level was performed to ensure that the amplitude range in the two data sets are comparable, at least in a qualitative way, in a 4D sense. We stress that with such significant differences between the data sets and their processing work flow it is the qualitative differences we can identify, such as a new amplitude distribution, and not a numerical value for a change in saturation or pressure. The RMS amplitude maps from Gas Level 2 from 1991 to 2005 are shown in Fig. 12.

The high resolution 2D lines were analyzed for time-shifts. The time-shifts down to the horizon corresponding to Gas Level 1 in Section 3.3 was measured from 1988 (before the blow out) to 1990 and 2009, respectively. This was done using a cross-correlation method where the maximum correlation time lag between the two traces, centered on a specific horizon, is assumed to be the time shift (e.g. Langseth and Landrø, 2012). Time-shifts down to a seismic horizon give information about changes that have occurred in the overlying sediments during the period between the data sets

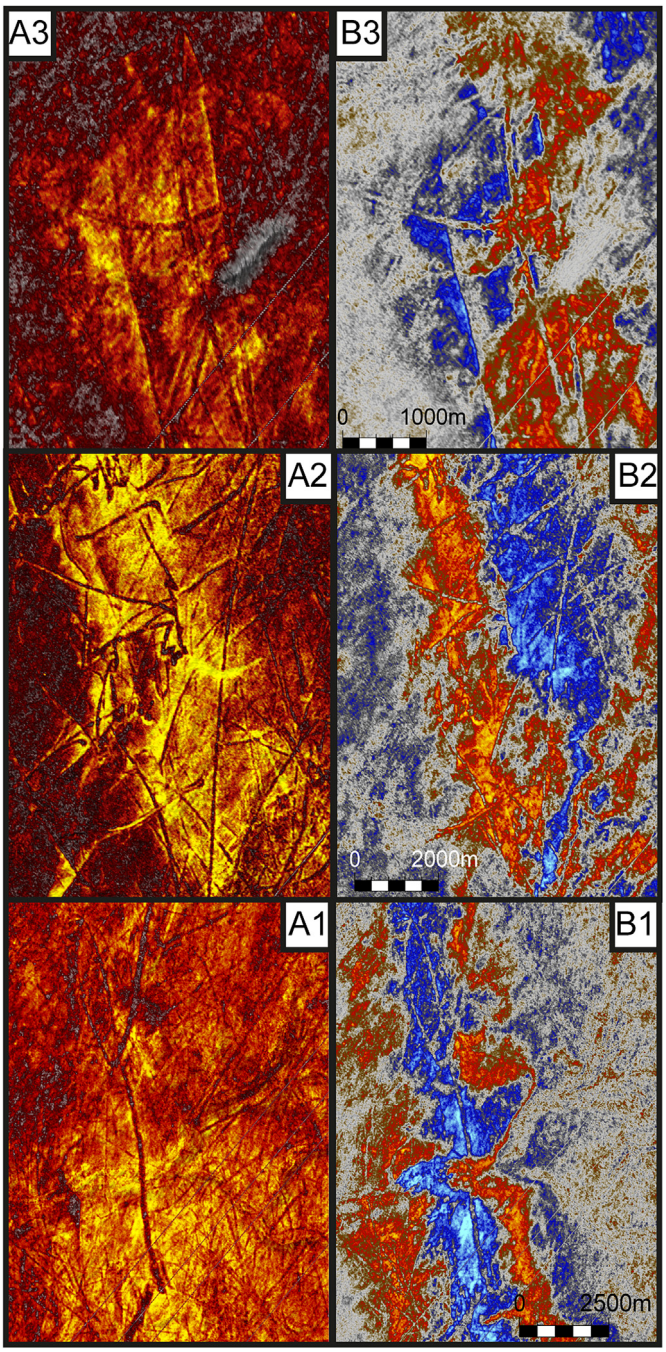

Fig. 8. Comparison of the detectability of linear to curve-linear features in the map generated from the different gas levels and time slices. The amplitude map from Gas Level 1 (A1) and a time slice at 680 ms (B1) from the position indicated in Fig. 5, in the 1991 3D data. (A2) and (B2) are the amplitude map from Gas Level 2 and a time-slice from 600 ms, respectively, from the position indicated in Fig. 6. (A3) and (B2) are the same as (A2) and (B2) for Gas Level 3. The position indicated in Fig. 7. The same color map is used in all amplitude maps.

were acquired, but do not give information about the exact depth of the change. The time-shifts are shown together with the position of the 2D line used for this analysis in Fig. 13.

3.6. Seismic response of thin sand layer

Tuning is the term used by the seismic interpretation community for interference between seismic reflections (e.g. Widess, 1953; Meissner and Meixner, 1969). If two reflectors, as the top and base of a sand layer, are closely spaced we would not necessarily be able to separate the two reflections in a seismic section. The appearance of the total seismic response from the two reflectors is dependent on the distance between the two reflectors and the frequency content of the seismic signal. Reyleygh's criterion for vertical resolution is a quarter of the wavelength λ of the dominant or peak frequency and often used as the resolution criteria in seismic (Sheriff, 1985), which is given as:

$$D_m = \frac{\lambda}{4} = \frac{\alpha}{4f_p}. \quad (1)$$

Where α is the P-wave velocity in the layer and f_p is the peak frequency of the seismic data. The vertical resolution above is defined as the limiting distance the reflectors have to be apart to still be resolved. The ability to resolve geological features is dependent on both resolution in time and space. The horizontal resolution is often taken as the 1. Fresnel diameter:

$$D = \sqrt{\frac{2z\alpha_{\text{avg}}}{f}} \quad (2)$$

where z is the depth down to the geology that is being imaged and α_{avg} is the average velocity down to z. For our 3D data set, if we assume $z = 600\ m$, $f_p = 45\ Hz$ and $\alpha_{avg} = 1900\ m/s$, the horizontal resolution is 110 m. However, the horizontal resolution in migrated 3D seismic data is about a quarter of the wavelength (Brown, 1999), but is dependent on noise and spatial sampling (Sheriff, 1985). The horizontal and vertical resolution in 3D data sets analyzed here, using these criteria, are both close to 10 m, and this corresponds to a temporal resolution of approximately 10 ms. This horizontal resolution is smaller than the bin cells in the 3D data, which means that the bin size will be the limiting factor controlling the horizontal resolution. Fig. 14 shows a comparison between the 1991 3D seismic and a high resolution 2D line from a site survey over one of the triangular shaped anomalies seen in Fig. 6A.

A wedge model consisting of a sand wedge in surrounding shale was generated. Seismic modeling using the convolution method was performed with a 45 Hz Ricker wavelet as source. Fig. 15 shows the seismic response of this wedge model, where the sand is saturated with 100% water in (B) and 12% gas in (C). The maximum amplitudes from the water and gas case are extracted and shown together with thickness of the wedge in (D). The velocities and densities used in Section 3.4, was also used in this model.

To test the detectability of iceberg ploughmarks in seismic data, a 2D finite difference modeling approach was used (e.g. Virieux, 1986) to generate synthetic seismic data. The model that was used had vertical sampling $\Delta z = 0.2$ m and horizontal sampling $\Delta x = 2$ m. A 45 Hz Ricker wavelet with sampling $\Delta t = 8^{*}10^{-5}$ s was used as source pulse. A line source was used to generate zero offset data. The data was then partially stacked in the horizontal direction to mimic binning, and then re-sampled to $\Delta x = 24$ m and $\Delta t = 4$ ms. This was done in order to resemble more realistic seismic acquisition. The data was then migrated using a post-stack Kirchhoff migration algorithm with a constant velocity. A 1D sinc interpolation was performed in order to make the synthetic seismic appears more similar to the seismic sections that are displayed in seismic interpretation softwares that are commonly used today. The models we use consist of a sand layer with 15 depressions in it that has the shape of a parabola. The width of the depressions were all 50 m, which equals the average width of ploughmarks earlier described in the early Pleistocene by Dowdeswell and Ottesen (2013), and the depths range from 1 to 15 m. Three different

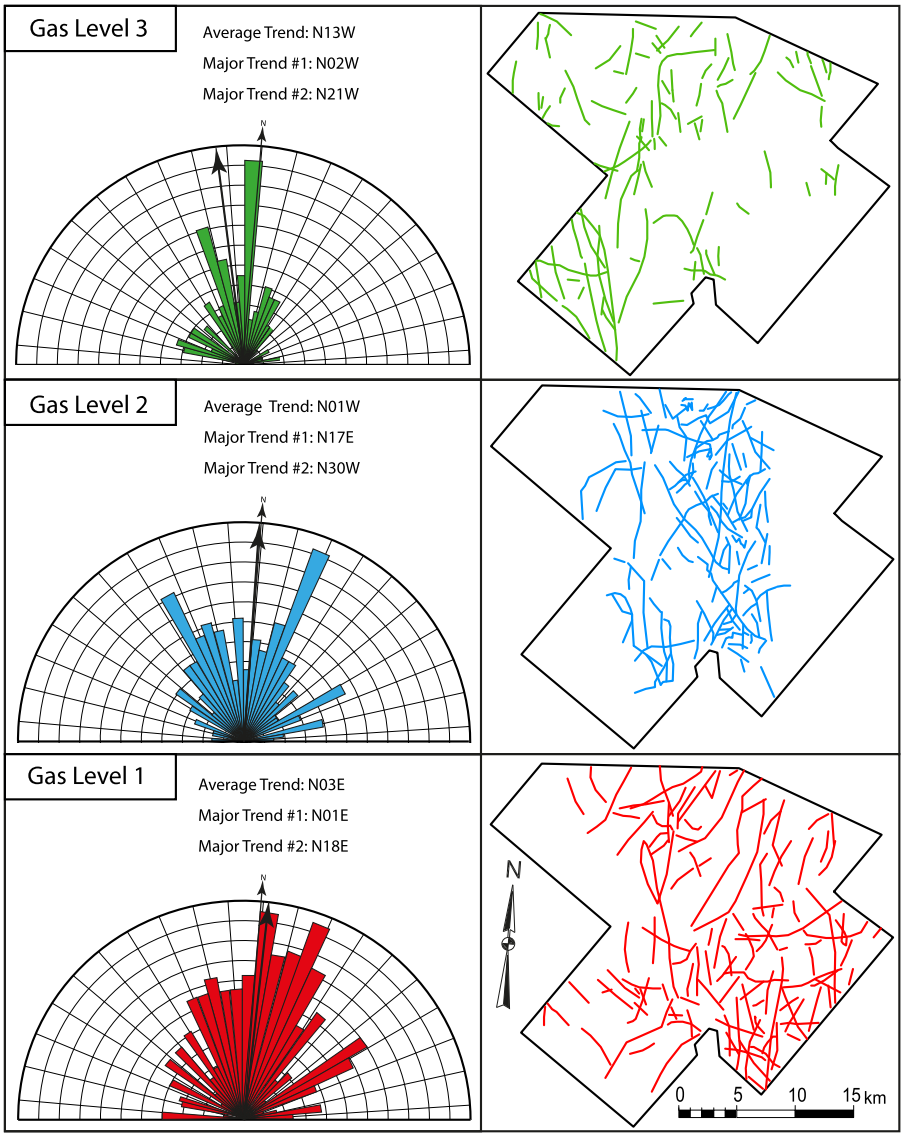

Fig. 9. The interpreted dim curve-linear to linear features with corresponding Rose diagrams showing the distributions of directions and average directions in black arrows for Gas Level 1, Gas Level 2 and Gas Level 3. The small black arrow in the rose diagrams shows where North is. The rose diagrams are only one-sided, but the measurements are uni-directional. The rose diagrams are weighted by the lengths of the ploughmarks.

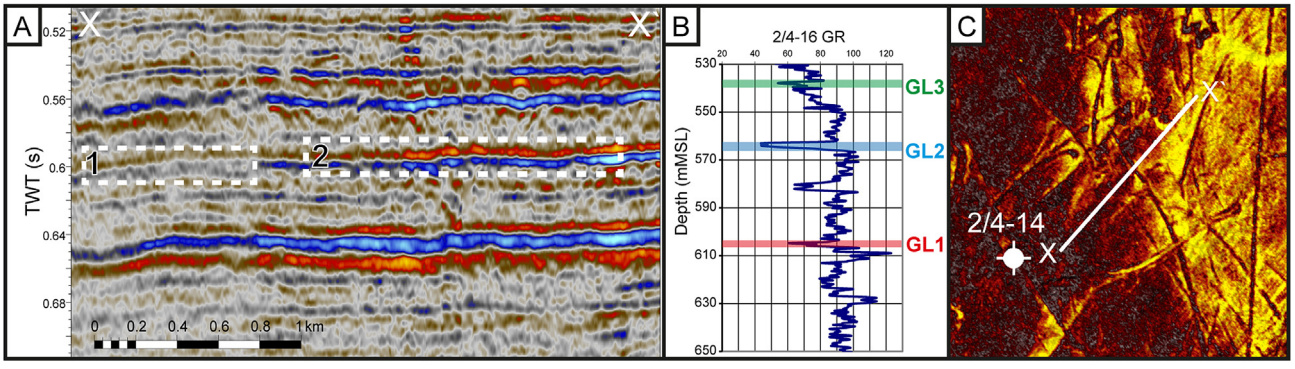

Fig. 10. (A) A shallow seismic profile showing the areas where AVO analysis has been performed. The presumed water filled and gas filled zones are indicated in Box 1 and 2, respectively. (B) Gamma ray log from the 2/4-16 well indicating sand layers around 530 m, 560 m, 580 m and 605 m. The colored intervals correspond to Level 1 (Red), Level 2 (Blue) and Level 3 (Green) in Section 3.3. (C) Part of the amplitude attribute map from Level 2 shown in Fig. 6 where the position of the seismic profile in (A) is indicated. Yellow indicates high amplitude and gray low.

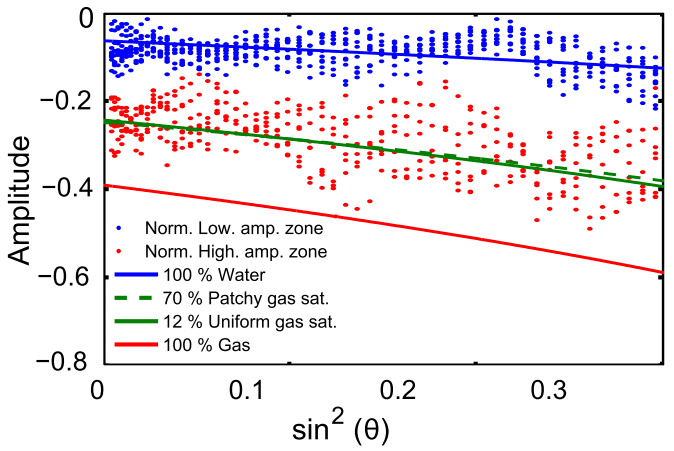

Fig. 11. AVO data from the low amplitude zone in Box 1 (Blue dots) and high amplitude zone in Box 2 (Red dots), in Fig. 10. The data has been corrected for geometrical spreading and attenuation and then normalized to the modeled AVO data as described in Section 3.4. The lines represent the modeled AVO response from an interface between two layers, shale above sand, where the sand has different saturations of gas and water, indicated by the legend.

thicknesses of the sand layer was modeled, 2 m, 6 m and 10 m, to see how tuning affect imaging of iceberg ploughmarks. RMS-amplitudes were then extracted in an 18 ms long window centered on the zero crossing of each of the migrated sections. Fig. 16 shows the modeled seismic response for the 15 depressions in sand layers of 2 m, 6 m, and 10 m.

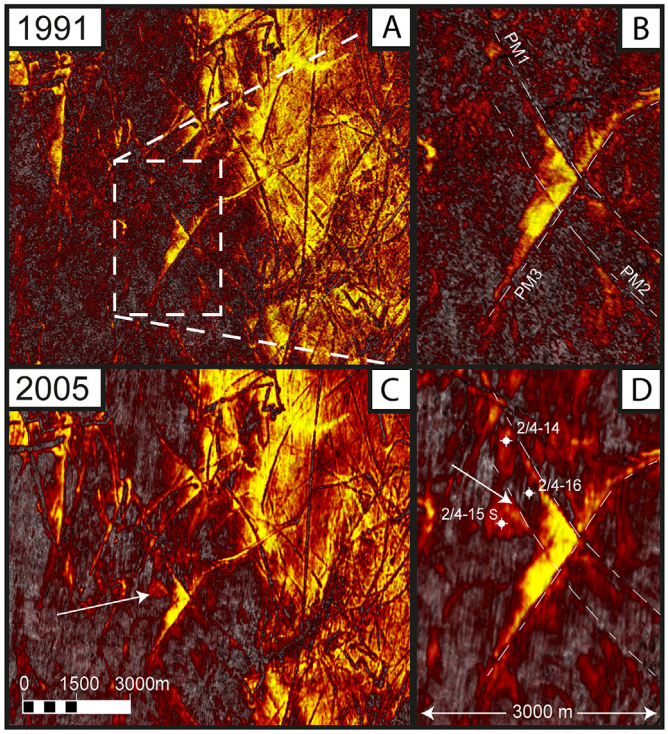

Fig. 12. (A) RMS amplitude map from Gas Level 2 extracted from the 1991 3D seismic data set. (B) Close up of the dashed white box in (A), showing a triangular shaped anomaly in vicinity of the 2/4-14 well. The thin dashed lines called PM1, PM2 and PM3 are interpretation of the dim curve-linear features that we see in the amplitude maps. (C) and (D) are the equivalents of (A) and (B), but for the 2005 3D data set. The position of the 2/4-14, -15 and -16 are indicated. An anomaly is present around the 2/4-15 well in (D) in the 2005 data set and is not present in the 1991 data set. This anomaly terminates towards the dashed line PM2 from (B) that are imposed onto (D), see white arrow.

2D finite difference modeling was also performed on a conceptual model of Gas Level 2. This result is shown in Fig. 18 and discussed in Section 5.

4. Results and interpretation

4.1. Regional stratigraphy

The Mid-Miocene Unconformity (MMU) is a high amplitude reflection in most of the North Sea. The overlying sediments of late Miocene and Pliocene are downlapping on the MMU reflection. The MMU horizon is the blue marker in Fig. 2. The Base Naust equivalent horizon is not a high amplitude or clear reflection in data set, but can be inferred from the downlapping of the latest Pliocene and early Pleistocene prograding delta sediments overlying this horizon, see orange marker in Fig. 2. The Upper Regional Unconformity equivalent is difficult to identify in the Central North Sea because the sediments above the URU are conformable with the URU. Our pick of the URU horizon is extrapolated from Fig. 4 in Anell et al. (2011) and is the purple marker Fig. 2. We are not very confident in our pick of the URU. The horizon called Gas Level 1 is a high amplitude horizon in our data set and is the red marker in Fig. 2.

In the regional profile in Fig. 2, we observe a vertical dim zone (indicated by arrow A) where the crossing horizons appear distorted. This zone cuts through the MMU and the Base Naust equivalent horizons, and appears to terminate above or below the Gas Level 1 horizon. We also observe anomalously high amplitude horizons, indicated with Arrow B, that extend up to 5 km away from this distorted vertical feature. We interpret this vertical distorted feature as a gas chimney, and the high amplitude anomalies extending out of this chimney as gas accumulations. We identify horizons that have higher amplitude than the surroundings in close vicinity of the top of the interpreted gas chimney. These horizons are brighter on the up-dip side (Northeast) of the gas chimney and we suggest that these are permeable sand layers that act as a migration route for gas. Possible entry points to the two horizons are indicated with Arrow C, and white arrows are positioned directly below these horizons in Fig. 2. We also observe over-deepened structures interpreted as tunnel valleys (arrow E in Fig. 2).

4.2. Iceberg ploughmarks

From the TWT map, in Fig. 4, we find that Gas Level 1 has an average dip of 0.3° towards West-Southwest, assuming an average velocity of 1900 *m/s* down to this horizon. Gas Level 2 and 3 have average dips of 0.2° in the same direction. The strike of the dips are 10°Northwest. An overburden velocity effect referred to as a pull-up can be observed in the TWT map in Fig. 4A. This pull-up is associated with high velocity tunnel valley infill in overlying early Quaternary sediments.

By studying the amplitude attribute maps in Figs. 5–7 we observe low amplitude linear to curve-linear features in a more high amplitude background. Some of the features exhibit a very predictive nature, while others have abrupt changes. Loops and cross-cuttings are also observed. These features exhibit the same appearance as iceberg ploughmarks that are observed at the modern high latitude shelves. These features are therefore interpreted to be buried iceberg ploughmarks. The interpretation of iceberg ploughmarks and the directional analysis (Fig. 9) show that the average trend of drifting icebergs was close to North-South for all three levels. However, we observe that the ploughmarks in Gas Level 2 can be described by two main trends, and that these trends are equally deviating away from the strike angle of the dip of the horizon with about 25°.

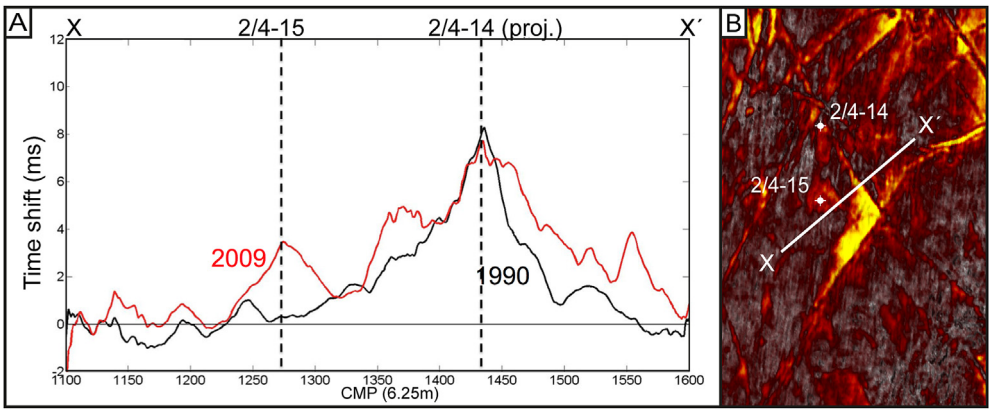

Fig. 13. (A) Time shifts to the reflector corresponding to Level 1, in Section 3.3, from before the blow out in 1988–1990 (black line) and 2009 (red line), respectively. The separation between the Common Mid Poitns (CMP) is 6.25 m, and the total profile is 2.5 km. These time-shifts are found from time-shift analysis of repeated high resolution 2D lines. The time-shifts seen at the projection (proj.) of the 2/4-14 well is due to the gas in the 490 m layer seen at approximately 550 ms in Fig. 3. We also observe an increased time-shift from 1990 to 2009 below the 2/4-15 well. (B) Part of the amplitude attribute map from Level 2 shown in Fig. 6. The position of the 2D line used for time-shift analyses is indicated by the white line, and the 2/4-14 and -15 wells are shown.

In the amplitude map from Gas Level 1 (Fig. 5), we observe a distribution of amplitudes that is highest around the Southernmost part of the white dashed box and then gradually decrease away. Dim lines can be seen across most of the map, but are more difficult to be interpreted or not visible in the westernmost part where the amplitudes are weak. The largest ploughmark is about 250 m wide and several individual ploughmarks have lengths that exceed 10 km (Fig. 5). The width of the ploughmark was measured between the high amplitudes, perpendicular to the dim line. This is shown in Fig. 5B.

The RMS amplitude map extracted from Gas Level 2 (in Fig. 6A) shows a different nature than Gas Level 1. We observe that the areas towards West and East are dim, and that there is a belt of high amplitudes in a trend that is close to the strike angle of the dip, and almost parallel to the line where the horizon truncates towards east (indicated by a dashed line and labeled “Truncation” in Fig. 6). This high amplitude belt stops towards West approximately at the dashed line labeled GWC in Fig. 6. High amplitude anomalies that are triangular in shape and positioned down-dip of cross-cutting dim curve-linear features are observed in the dimmer areas, West of the GWC line, and are indicated by arrows in Fig. 5A. We also observe high amplitude curve-linear events that occur in pairs, as seen in Fig. 6B, they have the same nature spatial nature as the ploughmarks that are interpreted from the dim linear features and are also interpreted as iceberg ploughmarks. The width of these high amplitude lines are up 60 m, when measuring between the low amplitude sides (opposite to Fig. 5B).

The RMS amplitudes from Level 3 (Fig. 7) are in general lower than the amplitudes observed in Gas Level 1 and 2. The nature of the amplitudes in Gas Level 3 is similar to those seen in Gas Level 1 in the upper half of the map, and a nature that is more equal to the triangular shaped anomalies observed in Gas Level 2 are observed in the white box in Fig. 7.

4.3. Amplitude versus offset analysis

We observe that the data points from the low amplitude zone (blue dots) and from the high amplitude zone (red dots) plot in separate regions in the amplitude vs. angle plot in Fig. 11. The reflection amplitudes from the high amplitude zone is more negative at zero offset and have a steeper gradient (i.e changing more rapidly with angle) than in the data from the low amplitude zone. This type of response is referred to as a class III AVO response (Rutherford and Williams, 1989), which is the typical AVO response for unconsolidated sands that are gas-bearing and below a harder shale. The scatter of data points observed in Fig. 11 is expected from real seismic data. Noise in the seismic data and small variations in geology and/or gas saturation at the different positions (CMPs) will cause this behavior. In the data set analyzed here we probably observe a combination of these effects.

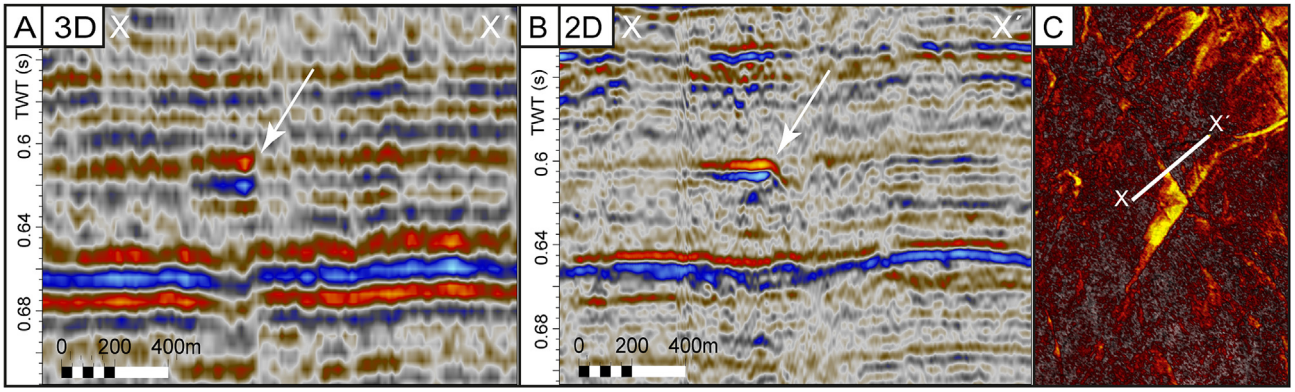

Fig. 14. Seismic sections across the triangular shaped anomaly in Level 2 from the SG9111 3D seismic cube in (A) and High resolution 2D line from the SG8910 survey in (B). (C) Amplitude map from Level 2 showing the triangular shaped anomaly and the position of the seismic sections in (A) and (B). The arrow indicates the position of the edge of the ploughmark in (A) and (B).

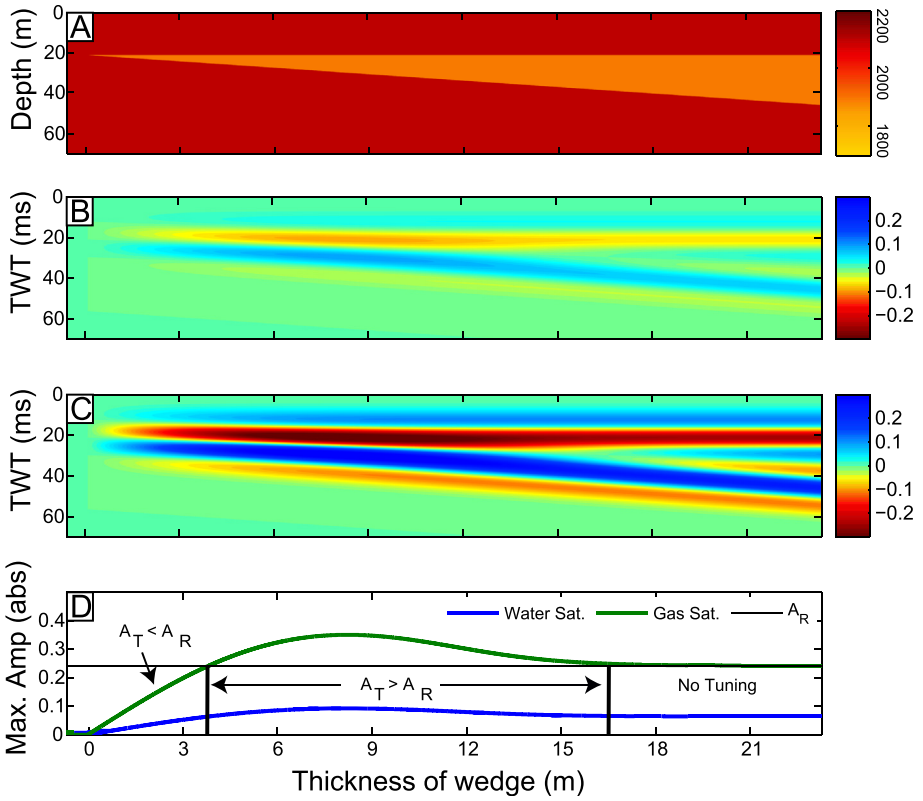

Fig. 15. (A) The P-wave velocity model used in modeling. The shale layer (red) is 2100 m/s and the velocity of the sand (orange) is 1900 m/s for water filled case and 1400 m/s for the gas case. The thickness of the sand is up to 23 m (B) Synthetic seismic of the water filled case. (C) Synthetic seismic for the gas filled case, with 12% uniform gas saturation as found from fluid substitution analysis described in Section 3.4. (D) The maximum amplitude from (B) and (C), and the thickness of the wedge versus the wedge X-position. A_T and A_R are the Tuning amplitude and the amplitude of a resolved separate reflection. When the thickness of the wedge is between 3.6 m and approximately 16.4 m, A_T is greater than the A_R. The difference in amplitude between the gas case and the water case significant for.

The modeled AVO responses for the simple model described in Section 3.4 are shown for different gas saturations and types of saturation in Fig. 11. The modeled response for 100% water saturated rock fit the data from the presumed water filled zone, which is expected because we normalized the data to the presumed water filled zone. However, the data is only normalized using a scalar and we still observe that the trend of the data fit the modeled AVO response very good. Modeling with 100% gas in the pores result in an AVO response that do not to fit the data points. We find that AVO Modeling with 12% uniform saturation or 70% patchy gas saturation gave best fit with the data from the high amplitude zone. The AVO analyses therefore indicate that the sand layer is partially saturated with gas where high amplitudes are observed, and that the saturation is somewhere in range from 12% to 70% depending on how the gas is distributed in the sand layer, patchy, uniformly or a combination.

4.4. Time-lapse analysis

RMS amplitude maps from Gas Level 2 (Section 3.3) are shown for both the 1991 and the 2005 3D seismic data sets in Fig. 12. The two maps are very similar in nature and the same dim linear to curve-linear crossing features can be recognized in both. We observe that the 2005 data set appears more smoothed and has less noise compared to the 1991 data set. The most obvious difference between the two maps is the new amplitude anomaly around the position of the 2/4-15 well, that is indicated with an arrow in Fig. 12C. We see that the triangle shaped anomaly appears brighter towards its easternmost margin and that it seems that the new high amplitude anomaly, around the 2/4-15 well, is stopping towards an interpreted iceberg ploughmark. This ploughmark is less visible in the 2005 data than the 1991 data, but can be inferred from the North-Northeast edge of the new high amplitude and from the dim line inside the triangular shaped anomaly, the interpreted ploughmarks are indicated by dashed white lines in Fig. 12 B and D. A new amplitude anomaly in a sand layer shows that the seismic velocity at this position in this layer has been lowered from 1991 to 2005, resulting in a higher reflection coefficient.

The time-shift analysis performed on the 2D high resolution line shows that the greatest time-shifts are located directly below the projection of the 2/4-14 well, see Fig. 13A. This time-shift is positioned below one of main recipients of gas from the 2/4-14 blow out positioned at 490 m below mean sea level, and has been studied previously (e.g. Lie and Larsen, 1991; Langseth and Landrø, 2012). This gas filled sand is indicated by Arrow D in Fig. 2. A larger time-shift can be observed below the 2/4-15 well in the period from 1988 to 2009 compared to the period 1988 to 1990. This implies that there has been a reduction in the velocity in the overlying sediments between 1990 and 2009. The observed time-shifts below the 2/4-15 well are up to 3 ms.

The time-shift below 2/4-15 suggest that there is a reduction in the velocity above Gas Level 1 and the new amplitude anomaly observed in Gas Level 2 shows that the velocity of the sand in Gas Level 2 has been reduced and the reflection strength has increased because of this. An interpretation that explain both of these observations is that gas from the 2/4-14 blowout has migrated up along the 2/4-15 well and entered Gas Level 2. However, if we attribute the maximum observed time-shift of 3 ms to a change in saturation in the 6 m thick sand layer, it implies a reduction of the velocity in the order of 900 m/s. A more sound interpretation is that

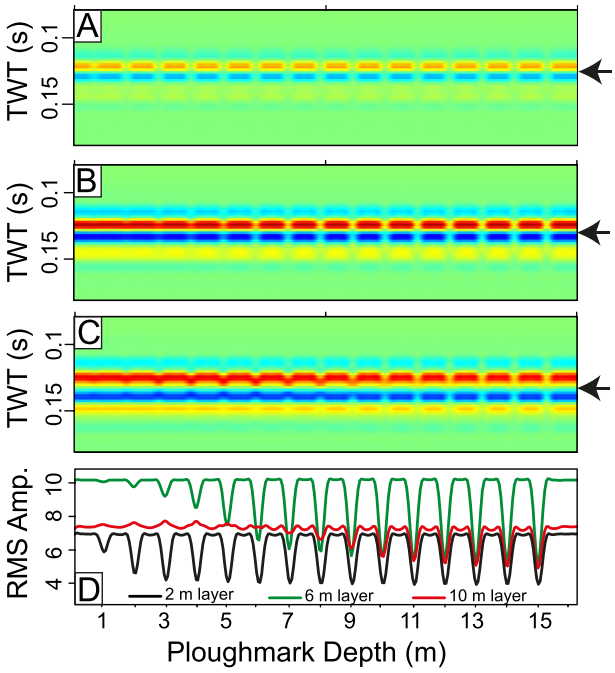

Fig. 16. (A), (B) and (c) are the migrated and interpolated synthetic seismic sections from thin sand layers that have 15 depressions in them ranging from 1 to 15 m. The widths of the depressions are all 50 m. The thickness of the sand layer is 2 m in (A), 6 m in (B) and 10 m in (C). The same color map is used in (A), (B) and (C). RMS amplitudes were extracted in an 18 ms window centered on the time indicated by the black arrows and are shown in (D).

gas from the 2/4-14 blowout has saturated thin sand layers and/or damaged formation around the 15 well in addition to charging Gas Level 2 with gas. Based on the data available, this fluid flow must have taken place between 1991 and 2005.

4.5. Seismic response of thin sand layer

The reflection response from a thin sand layer depends on its thickness and the frequency content of the seismic data. Fig. 15 shows that when the thickness of the sand layer is between 3.6 m and 16.4 m, its tuning amplitude A_T will be greater than the amplitude of a resolved top or base reflection, A_R, when using a 45 Hz Ricker wavelet. The tuning is independent of the fluid fill, but the amplitude will be proportional to the reflections coefficient. The reflection coefficient for the gas saturated case is 3.8 times as strong as for the water saturated case, and Fig. 15D shows that the response from gas filled sand layer, if it is thicker than 2 m, will be higher than the response from a water filled layer at maximum tuning thickness. Maximum tuning thickness for a Ricker wavelet with peak frequency $f_p = 45$ Hz occurs at 8.2 m. In Fig. 14 we observe that to the left of the high amplitude anomaly (indicated with arrows) we are able to continue interpret the high amplitude reflector, in both the data sets, where it dims to the left. This line very close to the 2/4-16 well where the sand layer is 6 m thick. Since this horizon can be interpreted where it is water filled, our tuning analysis suggests that we should be able to interpret, at least, a 2 m thick gas filled sand layer as well.

Modeling of depressions in thin sand layers show that iceberg ploughmarks that are 50 m wide can be visible in layers as thin as 2 m (Fig. 16A), using the method of extracting RMS amplitudes. When the sand layer is 6 m thick, its total response has a high amplitude, and the depressions can be spotted as dim zones if the if the ploughmark is deeper than 3 m and easily detected if the depth exceeds the layer thickness (Fig. 16B). Fig. 16C) shows that the detectability of iceberg ploughmarks will be reduced when the thickness of the layer is higher than maximum tuning thickness. However, at this thickness we start to see the depressions of the ploughmarks when they are deeper than 1 m.

The RMS amplitudes shown in Fig. 16D shows that the amplitude of the seismic signal at the position of iceberg ploughmarks are in general lower than the amplitude in surrounding, unaffected layer. However, by studying the RMS amplitudes extracted from the 10 m thick sand layer, we observe two things: When the depression is less than 4 m deep, there is an increase in amplitude and when the depression is deeper than 6 m there is an increase in amplitude on the edges of the depressions. These two observations can be explained by tuning effects. The 10 m thick layer is thicker than the maximum tuning thickness, and whenever a depression in the layer makes the layer thinner, its amplitude will increase.

5. Discussion

There may be several explanations for high amplitude horizons in a seismic section. Large contrasts in lithology or fluid fill between sedimentary layers will result in a high reflection coefficient and correspondingly bright reflectors in a stacked seismic image.

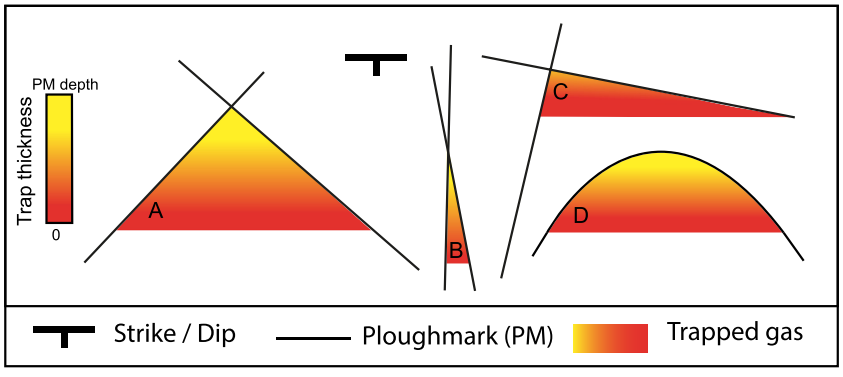

Fig. 17. This figure shows possible traps generated by iceberg ploughmarks seen from above. The strike (East-West) and dip (South) of the layer that the iceberg ploughmarks are situated in is indicated. The storage capacity of the traps created by the iceberg ploughmarks are related to the trend or trends of the ploughmarks relative to the strike of the dipping layer. When the angle between the trends of the ploughmarks and the strike angle are low, or relatively low as in (A) more gas can be trapped than if the angle is high as in (B). If the ploughmarks have trends that are very different compared to the strike angle, as in (C), it will lower the storage capacity compared to (A). Another possible trap can be wavy ploughmarks as in (D). The trap thickness or the height of the column of fluid it can trap is indicated by the color bar. The maximum height this type of trap can have is the depth of the ploughmark at its highest point (e.g. where the ploughmarks cross).

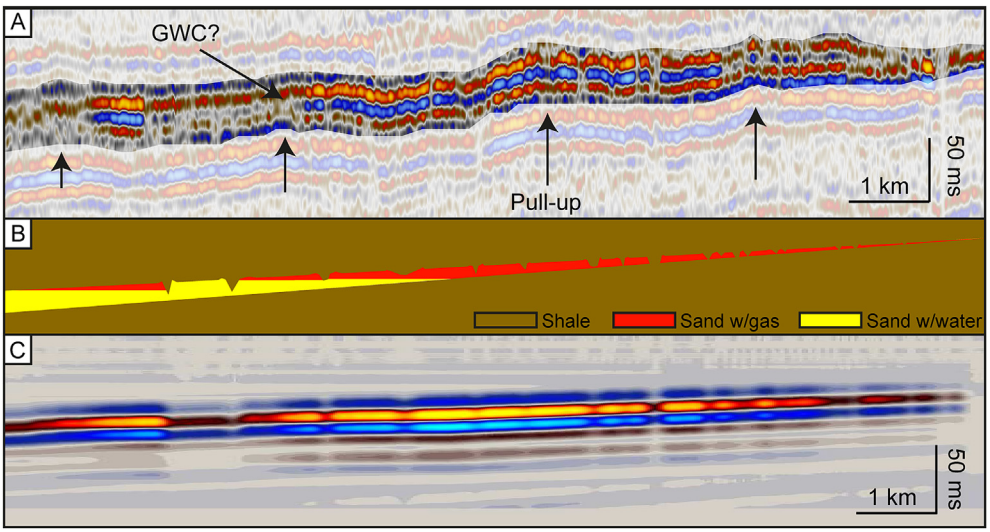

Fig. 18. (A) A random line from the SG9111 3D data set which position is indicated in Fig. 6. The line is running from Southwest towards Northeast from right to left. The reflection and close surroundings of Gas Level 2 are highlighted. The vertical arrows are indicating pull-ups in the seismic. The pull-ups are overburden velocity effects and make the apparent topography of the geology differ from its real. A possible gas to water contact is indicated with arrow GWC. (B) A conceptual model for Gas Level 2. A sand layer pinching out in surrounding shales and saturated with gas in two different traps; ploughmark trap and a stratigraphic trap. The sand layer is 7 m at its thickest (to left) and has several depressions that represent iceberg ploughmarks. (C) Synthetic migrated seismic section of the model in (B). The modeling procedure is explained in Section 3.6.

Examples of this can for example be sediments on bedrock, siliciclastic sediments on salt or hard carbonates, or sand/shale on coal. In this study, we present results that give good indications that the observed high amplitude horizons in the early Pleistocene sediments studied in this paper are due to gas accumulations in thin sand layers. AVO analyses show a clear separation between the data from the low amplitude and high amplitude zones (Box 1 and 2 in Fig. 10), and the AVO response from the high amplitude zone is a typical response from a gas saturated sand layer (Shuey, 1985; Rutherford and Williams, 1989; Avseth et al., 2005). Furthermore, time-lapse analysis indicate that gas from the 2/4-14 blowout been flowing into the sands of Gas Level 2 some time in the interval from 1991 to 2005 (Fig. 12). In addition to showing that gas from the 2/4-14 blow out has entered a new sand layer, it gives us a very good indication of how gas or hydrocarbons in Gas Level 2 appears in seismic. The fact that the new gas accumulation exhibits the same nature as the surrounding anomalies, strengthens our interpretation that the observed high amplitude anomalies in the studied interval are related to shallow gas.

The seismic modeling show that iceberg ploughmarks should be detectable in seismic data is dim features, and that ploughmarks should be observable in layers as thin as 2m. A factor that influences the ability to detect the ploughmarks is the depth of the ploughmark. If the depth of ploughmark exceeds the thickness of the sand layer it is positioned in, it will be very detectable in RMS amplitude maps. The modeling shows that when the layer is thicker than the depth of the ploughmark it is reducing the detectability (Fig. 16). The Noise level in the seismic data set will also have an impact on the detectability of iceberg ploughmarks. We can not detect variations that are smaller than the noise level. Extracting RMS values in a window is a stacking method that will enhance coherent signal and reduce non-coherent noise, and will increase the differences between high and low amplitude zones in the horizon under investigation.

The triangular shaped anomalies observed in Gas Level 2 (Fig. 6) have earlier been interpreted as a result of relict ploughmarks acting as a trapping mechanism for shallow gas (Haavik and Landrø, 2013). This trap is the result of icebergs that have plowed down in a sandy sea floor, followed by deposition of finer sediments that can act as a seal, or that the icebergs have plowed down in sand that lies beneath shale. To form a trap, two of the ploughmarks must cross each other or one ploughmark must be part of an ellipse or a semicircle (Fig. 17). The sandy layer must, at least, locally, have a dip to generate volume where gas can be trapped. Furthermore, we think that the angle between the trend of the iceberg ploughmarks and the strike of the dipping layer should be close, but not equal, to give the traps a large storage potential. If the trend of the ploughmarks are close to perpendicular to the strike of the dip the storage potential will be lower, see Fig. 17. The dim lines The parallel high amplitude lines, shown in Fig. 6B, must have a different explanation. The modeling suggest that an increase in amplitude will occur when an iceberg ploughmark decreases the total thickness of a layer into tuning thickness (Fig. 16D), but this increase appears to be in the order of a few percent and cannot explain the observations. The parallel high amplitude lines are in a low amplitude background and the RMS amplitude from these features are ranging from 2 to 5 times as high as the background amplitude. This suggests that the surroundings are water filled, while the high amplitude lines are gas filled. An explanation for this can be that the ploughmarks have berms that are high enough to trap gas and wide enough to be observed. In that case, the width of the berms can be over 60 m wide. This explains why the lines are parallel too; that berms are positioned on both sides of the depression.

The reason why we see this sort of trap in Gas Level 2 is probably a combination of several factors. The ploughmarks observed in this layer have two main directional trends and these trends have the same small deviation from the strike of the dip, giving the traps a good storage potential. The gamma ray response from the layer corresponding to Gas Level 2 is low compared to that of Gas Level 1 and 3 (Fig. 10C). This is indicating that this sand layer is cleaner than the other layers. Clean and poorly consolidated sandstones are usually correlated with high permeability and porosity (Nelson, 1994), and this means that the sands of Gas Level 2 may act as an effective migration route for the gas. The gas traps will appear very strong and stand out from the surroundings if less gas is trapped in heterogeneities inside the sand layer.

Our interpretation is that the sand layer of Gas Level 2 is pinching out towards East and form a reservoir that is filled with

gas. We interpret the GWC line in Fig. 6 to be the approximate gas-water contact. When gas has entered the sand layer of Gas Level 2, it has migrated up-dip towards Northeast. Some of the gas gets trapped in the smaller triangular shaped anomalies discussed above, and the rest is filling the stratigraphic trap. This shallow gas reservoir appears to extend out of the 3D data set available for this study, at least to the North. Fig. 18A shows a seismic line running perpendicular to the belt of high amplitudes and also across one of the triangular shaped anomalies, and the reflector of Gas Level 2 is highlighted. A schematic model for how the gas is trapped in Gas Level 2 is shown in Fig. 18B and synthetic seismic of this model is shown in Fig. 18C.

The regional seismic profile in Fig. 2 indicates that the shallow gas observed in Gas Level 1, Gas Level 2 and Gas Level 3 has been sourced from deeper strata, with the exception of the gas from the 2/4-14 blowout, and therefore has thermogenic origin. Vertical gas migration can be inferred from the interpreted gas chimney and we think that horizontal migration occurred through the observed high amplitude shallow sandy layers (see Fig. 2). However, we do not exclude the possibility that parts of the gas have biogenic origin. We have not discussed the possibility that the sand layers studied here are filled with oil. These sand layers are very thin and an oil response might not been detected by well logs, but they have a huge extent. The belt of high amplitudes in Gas Level 2 has an area over 570 km^2 in this data set, and appears to continue further out of the data set. The conceptual model in Fig. 18 may be a new, far-fetched, Quaternary exploration play model in the Central North Sea.

The iceberg ploughmarks that have been identified in this paper are positioned between roughly 470 m and 700 m below mean sea level and positioned above the interpreted Base Naust equivalent horizon (Fig. 2), and the directional trend of the iceberg ploughmarks in this data set is consistent with the observations in Stuart and Huuse (2012) and Dowdeswell and Ottesen (2013). In the Central North Sea the Base Naust equivalent horizon is about 2.7 Ma and have been correlated to the 2/4-C-11 well at approximately 700 m depth in Ottesen et al. (2014) and 980 m in Eidvin et al. (1999) and (Eidvin et al., 2013). The 2/4-C-11 well is positioned 12 km South of the 2/4-14 well and its position is indicated in Fig. 4 right outside the 3D seismic data set available for this study. Our interpretation of the Base Naust equivalent horizon at the 2/4-14 well gives a depth below mean sea level of roughly 950 m, when using an average velocity of 1900 m/s down to this horizon. This is in good correspondence with the depth from Eidvin et al. (1999). However, there is an ambiguity in the depth of the Base Naust equivalent in this study and Eidvin et al. (1999) and to the one in Dowdeswell and Ottesen (2013) and Ottesen et al. (2014). This ambiguity makes it difficult to date the iceberg ploughmarks identified here. By using the depth of the Base Naust equivalent horizon from Fig. 4 in Ottesen et al. (2014) we find that the ploughmarks identified in this study can be as old as 2.7 Ma. If we compare the horizon that corresponding to Gas Level 1 in Fig. 2 to earlier interpretations from this area, Fig. 6 in Huuse (2002) and Fig. 4 in Michelsen (2001), we find that the ploughmarks should be close to 1.8 Ma based on their interpretation. In comparison, about 200 km further to the South, Kuhlmann and Wong (2008) described an interval heavily influenced by iceberg plowing which they dated to be around 1.9 Ma. A more detailed stratigraphic study is needed to date the interval properly.

Eidvin et al. (1999) found small quantities of ice-rafted material in the cores and cuttings in the early Pleistocene section of the 2/4-C-11 well compared to sediments at comparable depths in the northern North Sea. This was interpreted as if this area was less influenced by icebergs than the areas in the Northern North Sea. In contrast to Eidvin et al. (1999) findings, (Dowdeswell and Ottesen, 2013) and this study show that the early Pleistocene sediments in the Central North Sea are heavily influenced by icebergs.

The sediments of the Naust Formation in the Central North Sea are fine grained, probably distal deposits from fluvial and glacio-fluivial sources in South and Southeast (Ottesen et al., 2014), and the ploughmarks observed in the Central North Sea are probable formed in relatively deep water (Dowdeswell and Ottesen, 2013). In this study we find multiple thin sand layers in the Naust formation, and that these layers are embedded in finer sediments that are sealing. These sands have probably been deposited in deep water, and we speculate that sediment failure in the delta fronts of the fluvial systems to the South and Southeast are the sources of these sands. The sand layers may have been covered in finer sediments prior to the generation of the ploughmarks, as long as the ploughmarks are deep enough to penetrate into the sands we should be able to observe them in seismic. The three different layers may therefore be a result of periods with very high sedimentation rates causing the delta front instabilities (Adams and Roberts, 1993; Benvenuti et al., 2012).

The method for detecting iceberg ploughmarks using time-slices through the seismic data have shown great results (e.g. Dowdeswell and Ottesen, 2013). However, a shortcoming of that method is that it is not able to correctly resemble a palaeo-seafloor, especially if the layers under investigation have topography or are affected by overburden velocity effects (e.g. pull-ups as seen in Fig. 4). The choice of method for detecting iceberg ploughmarks should be based on the topography in the area. It is clear, from the comparison made in Fig. 8, that the method of time-slicing is able to detect buried ploughmarks in this area. However, by manually picking horizons, we assure that the interpreted iceberg ploughmarks are roughly of the same age. We are also able to interpret more iceberg ploughmarks because of this.

We have shown that conventional picking of seismic reflectors followed by amplitude attribute analysis can give beautiful images where iceberg ploughmarks can easily be detected. The method works very well where gas is illuminating shallow sand layers giving locally high amplitude horizons in the seismic. This method is extremely fast using auto tracking algorithms that are available in most of the seismic interpretation soft wares used today. Using the described method on a larger data set may give insight into the spatial and temporal distribution of iceberg ploughmarks through a larger sediment record. This may in provide further insight into glaciations of the early Pleistocene.

6. Conclusions

- Sandy layers probably deposited in deep water during early Pleistocene are visible as high amplitude horizons in seismic data. The high amplitudes are associated with gas in these layers. This is supported by geophysical analysis and seismic interpretation.
- By picking these high amplitude sandy layers in 3D seismic data and performing amplitude attribute analysis we obtain maps where iceberg ploughmarks can easily be detected as dim linear to curve-linear features, showing that the sandy layers was deposited under glacial influence.
- For the three early Pleistocene sand layers studied here we find that the iceberg ploughmarks have a principal direction in a close to a North-South trend. The age of these ploughmarks is probably around 1.8 Ma.
- AVO-analysis confirms that high amplitude anomalies are most likely caused by the presence of shallow gas.
- The shallow gas present in the sand layers under investigation is most likely of thermogenic origin, and a result of migration from deeper layers.

- Two types of hydrocarbon traps are observed in this data set. One of the traps is a stratigraphic pinch out. The other trap is a result of buried iceberg ploughmarks, and is to our knowledge, the only place where this type of trap has been documented.
- Gas from the 2/4-14 blowout in 1989 has migrated further into a new sand layer from 1991 to 2005.

Acknowledgments

We would like to thank Kjersti Eidissen for processing the AVO data used in this study. We acknowledge the Norwegian Research Council for financial support to the Rose project at NTNU. We acknowledge the sponsors of the Long term seismic monitoring (LOSEM) project for financial support: BayernGas, BP, CGG, Det Norske, Lundin Norway, Petrobras, Statoil and Total. We acknowledge Lundin Norway AS for financial support for Kjetil E. Haavik's PhD Project. We also acknowledge Dag Ottesen for valuable advice and feedback. Furthermore, the reviewers, Helge Løseth and Margaret A. Stewart, are acknowledged for useful comments and suggestions that improved this manuscript.

Appendix A. Amplitude versus offset modeling

The equations used in AVO-modeling are presented in this Appendix.

Appendix A.1Angle dependent reflection coefficients

Amplitude versus offset analysis is a method where angle dependent reflection-coefficients are used to make inferences about the rock properties, mineralogy and fluid content. Reflection coefficients that vary with angle is an effect of the energy distribution over a boundary. By imposing the boundary conditions that two layers have welded contact, Zöppritz (1919) derived the equations for how the energy from an incident wave will be distributed in reflected, transmitted and converted waves. A widely used approximation to the Zöppritz equations for P-wave reflection was given by Shuey (1985) as:

$$R(\theta) = R(0) + G\sin^2(\theta) + F\tan^2(\theta)\sin^2(\theta) \tag{A.1}$$

where:

$$R(0) = \frac{1}{2}\left(\frac{\Delta\alpha}{\overline{\alpha}} + \frac{\Delta\rho}{\overline{\rho}}\right) \tag{A.2}$$

$$G = \frac{1}{2}\frac{\Delta\alpha}{\overline{\alpha}} - \frac{2\overline{\beta}^2}{\overline{\alpha}^2}\left(\frac{2\Delta\beta}{\overline{\beta}} + \frac{\Delta\rho}{\overline{\rho}}\right) \tag{A.3}$$

$$F = \frac{1}{2}\frac{\Delta\alpha}{\overline{\alpha}} \tag{A.4}$$

and $\overline{x} = (x_1 + x_2)/2$, $\Delta x = x_2 - x_1$ for $x_i = \alpha_i, \beta_i, \rho_i$ where subscript i indicate the layer number. We see that the P-wave velocity α, S-wave velocity β and density ρ for both layers are needed to model the angle dependent reflection coefficient given in Eq. (A.1).

Appendix A.2Gassman fluid substitution

Fluid substitution is done, using the equations given by Gassman (1951), to predict the effective elastic moduli, or velocities, of a porous and permeable rock saturated with different fluids. In order to perform fluid substitution we need to know the S-wave velocity β, P-wave velocity α, density ρ, porosity ϕ and bulk modulus of the solid K_s and the fluid saturating the pores K_{f_1}. Furthermore, the Bulk modulus and density of the fluid we would like to saturate the rock with are required. The procedure is given by e. g Avseth et al. (2005):

1. Find the effective bulk and shear moduli from velocities and density for a rock saturated with a fluid 1, here indicated by subscript 1:

$$K_1 = \rho_1\left(\alpha_1^2 + \frac{4}{3}\beta_1^2\right) \tag{A.5}$$

$$\mu_1 = \rho_1\beta_1^2 \tag{A.6}$$

2. Use the equations from Gassman (1951) to find the bulk modulus to the rock saturated with fluid 2, K_2:

$$\frac{K_2}{K_s - K_2} - \frac{K_{f_2}}{\phi\left(K_s - K_{f_2}\right)} = \frac{K_1}{K_s - K_1} - \frac{K_{f_1}}{\phi\left(K_s - K_{f_1}\right)} \tag{A.7}$$

3. According to Biot theory the shear modulus μ remain unchanged.

$$\mu_2 = \mu_1 \tag{A.8}$$

4. Calculate the bulk density of the rock saturated with fluid 2.

$$\rho_2 = \rho_1 + \phi\left(\rho_{f_2} - \rho_{f_1}\right) \tag{A.9}$$

5. Calculate the velocities for the rock saturated with fluid 2.

$$\alpha_2 = \sqrt{\frac{K_2 + \frac{4}{3}\mu_2}{\rho_2}} \tag{A.10}$$

$$\beta_2 = \sqrt{\frac{\mu_2}{\rho_2}} \tag{A.11}$$

These velocities can then be used in e.g. AVO-modeling.

Appendix A.3Bulk modulus and density of fluid mixtures

Often the gas or oil saturation in rocks are not 100%. To model the properties of fluids that consist of more than one phase we use averages. For gas solved in water it is often assumed that the two phases experience the same pressure when a seismic wave propagate through it and the effective bulk modulus can be given by the "iso-stress" or Reuss average (Avseth et al., 2005):

$$K_{f_m}^R = \left(\frac{S_{f_1}}{K_{f_1}} + \frac{S_{f_2}}{K_{f_2}}\right)^{-1} \tag{A.12}$$

Where K_{f_m}, K_{f_1} and K_{f_2} are the bulk modulus of the mixture of fluids given by Reuss average, the bulk modulus of fluid 1 and the bulk modulus of fluid 2, respectively. S_{f_1} and S_{f_2} are the amount of fluid 1

and fluid two each fluid and $S_{f_1} + S_{f_2} = 1$. The average given in Eq. (A.12) is often used for gas solved in water, i. e uniformly mixed fluids. However, the geometrical distribution of the gas may be quite different in nature. If the gas is distributed as larger patches in a background of water then another average is often used, the Voigt average:

$$K_{f_m}^V = S_{f_1} K_{f_1} + S_{f_2} K_{f_2} \tag{A.13}$$

The average given in Eq. (A.13) is used when the patches of gas are on a scale that is larger than a critical scale (Mavko and Mukerji, 1998). This critical scale is dependent on the permeability of the rock, bulk modulus and viscosity of the fluid, and the frequency of the seismic (wavelength). Mavko and Mukerji (1998) find that the use of Eq. (A.13) in fluid substitution gives good results for patchy saturation.

The density of the fluid mixture is given for both uniform and patchy saturation mixtures as:

$$\rho_{f_m} = S_{f_1} \rho_{f_1} + S_{f_2} \rho_{f_2} \tag{A.14}$$

The density ρ_{f_m} and bulk moduli $K_{f_m}^R$ or $K_{f_m}^V$ are used in fluid substitution depending on the type of saturation, i. e the mixture of fluids. When free gas is present in the system, patchy saturation is likely to occur (Sengupta, 2000).

Appendix A.4Empirical relationships for S-wave velocity and density

Often we do not have all the parameters that are required for AVO modeling. We then rely on empirical relations that can give us estimates of the unknown parameters through the parameters we know. To get an estimate of S-wave velocity β in both layers, we used the empirical relationship given by Han (1986) which uses P-wave velocity α as input:

$$\beta = 0.793\alpha - 786.8 \tag{A.15}$$

This empirical relationship is found for clean unconsolidated sandstones at 40 MPa confining pressure.

The density for a brine saturated poorly consolidated sandstone is here estimated by the use of the density of Quartz ρ_Q and brine ρ_w together with an assumed porosity ϕ.

$$\rho = \rho_Q(1 - \phi) + \rho_w\phi. \tag{A.16}$$

Another way of estimating the density is through the empirical relationship from Gardner et al. (1974), who found that the density can be estimated using the P-wave velocity α as:

$$\rho = 0.23\alpha^{0.25}. \tag{A.17}$$

References

Adams, C.E.J., Roberts, H.H., 1993. A model of the effects of sedimentation rate on the stability of mississippi delta sediments. Geo-Mar. Lett. 13, 17–23.

Anell, I., Thybo, H., Rasmussen, E., 2011. A synthesis of Cenozoic sedimentation in the North Sea. Basin Res. 23, 1–26.

Arntsen, B., Wensaas, L., Løseth, H., Hermanrud, C., 2007. Seismic modeling of gas chimneys. Geophysics 72, SM251–SM259.

Avseth, P., Mukerji, T., Mavko, G., 2005. Quantitative Seismic Interpretation. Cambridge University Press.

Benvenuti, K., Kombrink, H., ten Veen, J.H., Munsterman, D.K., Bardi, F., Benvenuti, M., 2012. Late Cenozoic shelf delta development and mass transport deposits in the Dutch offshore area results of 3D seismic interpretation. Neth. J. Geosci. 91, 591–608.

Bijlsma, S., 1981. Fluvial sedimentation from the fennoscandian area into the North-West european Basin during the Late Cenozoic. Geol. Mijnb. 60, 337–345.

Bjørlykke, K., 2011. Petroleum Geoscience: from Sedimentary Environments to Rock Physics. Springer Vorlag.

Brown, A.R., 1999. Interpretation of Three-dimensional Seismic Data, vol. 42. AAPG.

Cameron, T.D.J., Bulat, J., Mesdag, C.S., 1993. High resolution seismic profile through a late Cenozoic delta complex in the southern North Sea. Mar. Pet. Geol. 10, 591–599.

Cameron, T.D.J., Stoker, M.S., Long, D., 1987. The history of Quaternary sedimentation in the UK sector of the North Sea. J. Geol. Soc. 144, 43–58.

Clark, C.D., Hughes, A.L.C., Greenwood, S.L., Jordan, C., Sejrup, H., 2012. Pattern and timing of retreat of the last British-Irish Ice Sheet. Quat. Sci. Rev. 44, 112–146.

Dalland, A., Worsley, D., Ofstad, K., 1988. A lithostratigraphic scheme for the Mesozoic and Cenozoic succession offshore mid- and northern Norway. NPD Bull. No., 4.

Davis, A.M., 1992. Shallow gas: an overview. Cont. Shelf Res. 12, 1077–1079.

Deegan, C.E., Scull, J.B.C., 1977. A standard lithologic nomenclature for the Central and Northern North Sea. Institute of Geological Sciences Report 77/25 NPD Bull. 1.

D'Heur, M., 1987. "Albuskjell":Geology of Norwegian Oil and Gas Fields North Sea. Graham and Trotman, Ltd.

Dowdeswell, J.A., Forsberg, C.F., 1992. The size and frequency of icebergs and bergy bits derived from tidewater glaciers in Kongsfjorden, northwest Spitsbergen. Polar Res. 11, 81–91.

Dowdeswell, J.A., Ottesen, D., 2013. Buried iceberg ploughmarks in the early Quaternary sediments of the central North Sea: a two-million year record of glacial influence from 3D seismic data. Mar. Geol. 344, 1–9.

Dowdeswell, J.A., Villinger, H., Whittington, R.J., Marienfield, P., 1993. Iceberg scouring in Scoresby Sund on the east Greenland continental shelf. Mar. Geol. 111, 37–53.

Ehlers, J., 1990. Reconstructing the dynamics of the North-west European Pleistocene ice sheets. Quat. Sci. Rev. 9, 7183.

Ehlers, J., Gibbard, P.L., 2008. Extent and chronology of Quaternary glaciation. Episodes, Geol. Soc. India 31, 211–218.

Eidvin, T., Riis, F., Rasmussen, E.S., Rundberg, Y., 2013. Investigation of Oligocene to lower pliocene deposits in the Nordic area. NPD Bull. No., 10.

Eidvin, T., Riis, F., Rundberg, Y., 1999. Upper Cainozoic stratigraphy in the Central North sea (Ekofisk and Sleipner fields). Nor. Geol. Tidsskr. 79, 97–128.

Floodgate, G.D., Judd, A.G., 1992. The origin of shallow gas. Cont. Shelf Res. 12, 1145–1156.

Gallagher, J.W., Heggland, R., 1994. Shallow gas evaluations based on conventional 3-D seismic data. In: 56th EAGE Conference and Exhibition, Vienna.

Gardner, G.H.F., Gardner, L.W., Gregory, A.R., 1974. Formation velocity and density the diagnostic basics for stratigraphic traps. Geophysics 39, 770–780.

Gassman, F., 1951. Über die Elastizitat poroser Medien. Veirteljahrsschrift der Naturforschen den Gesellschaft Zürich 96, 1–23.

Gatliff, R.W., Richards, P.C., Smith, K., Graham, C.C., McCormac, M., Smith, N.J.P., Long, D., Cameron, T.D.J., Evans, D., Stevenson, A.G., Bulat, J., Ritchie, J.D., 1994. UK Offshore Regional Report: the Geology of the Central North Sea. British Geological Survey.

Gibbard, P.L., 1988. The history of the great northwest European rivers during the past three million years. J. Quat. Sci. 318, 559–602.

Gibbard, P.L., Head, M., Walker, M.J.C., The subcommision on Quaternary Stratigraphy, 2010. Formal ratification of the Quaternary System Period and the Pleistocene Series Epoch with a base at 2.58 Ma. Phil. Trans. Royal Soc. Lond. 25, 96–102.

Graham, A.G.C., Lonergan, L., Stoker, M.S., 2007. Evidence for Late Pleistocene ice stream activity in the Witch Ground Basin, central North Sea, from 3D seismic reflection data. Quat. Sci. Rev. 26, 627–643.

Graham, A.G.C., Lonergan, L., Stoker, M.S., 2010. Depositional environments and chronology of Late Weichselian glaciation and deglaciation in the central North Sea. Boreas 39, 471–491.

Graham, A.G.C., Stoker, M.S., Lonergan, L., Bradwell, T., Stewart, M.A., 2011. The Pleistocene glaciations of the North sea Basin. In: Ehlers, J., Gibbard, P.L., Hughes, P.D. (Eds.), Quaternary Glaciations : Extent and Chronology : a Closer Look, Developments in Quaternary Science, vol. 15, pp. 261–278.

Granli, J.R., Arntsen, B., Sollid, A., Hilde, E., 1999. Imaging through gas-filled sediments using marine shear-wave data. Geophysics 64, 668–677.

Greaves, R., Fulp, T., 1987. Threedimensional seismic monitoring of an enhanced oil recovery process. Geophysics 52, 1175–1187.

Haavik, K., Landrø, M., 2013. Ice scours as trapping mechanism for shallow gas. In: 75th EAGE Conference and Exhibition Incorporating SPE EUROPEC, London.

Hampson, D., Russell, B., 1990. AVO Inversion: Theory and Practice. SEG Technical Program Expanded Abstracts, pp. 1456–1458.

Han, D.-H., 1986. Effects of Porosity and Clay Content on Acoustic Properties of Sandstones and Unconsolidated Sediments. Ph.D. thesis. Stanford University.

Heggland, R., 1998. Gas seepage as an indicator of deeper prospective reservoirs. A study based on exploration 3D seismic data. Mar. Pet. Geol. 15, 1.

Huuse, M., 2002. Cenozoic uplift and denundation of southern Norway: insights from the North Sea Basin. Geol. Soc. Lond. Spec. Publ. 196, 209–233.

Huuse, M., Lykke-Andersen, H., Michelsen, O., 2001. Cenozoic evolution of the eastern North Sea Basin new evidence from high-resolution and conventional seismic data. Mar. Geol. 177, 243269.

Jansen, E., Sjøholm, J., 1991. Reconstruction of glaciation over the past 6 Myr from ice-borne deposits in the Norwegian Sea. Nature 349, 600–603.

Jordt, H., Faleide, J.I., Bjørlykke, K., Ibrahim, M.T., 1995. Cenozoic sequence stratigraphy of the central and northern North Sea: tectonic development, sediment distribution and provenance area. Mar. Pet. Geol. 12, 845–879.

Judd, A.G., Hovland, M., 1992. The evidence for shallow gas in marine sediments. Cont. Shelf Res. 12, 10811095.

Kuhlmann, G., Wong, T.E., 2008. Pliocene Paleoenvironment evolution as interpreted from 3D-seismic data in the southern North Sea, Dutch offshore sector. Mar. Pet. Geol. 25, 173–189.
Landrø, M., 2001. Discrimination between pressure and fluid saturation changes from timelapse seismic data. Geophysics 66, 836–844.
Landrø, M., 2011. Seismic monitoring of an old underground blowout – 20 years later. First Break 29, 845–879.
Landrø, M., Solheim, O.A., Hilde, E., Strnen, L.K., 1999. The Gullfaks 4D seismic study. Pet. Geosci. 5, 213–226.
Langseth, E., Landrø, M., 2012. Time-Lapse 2D interpretation of gas migration in shallow sand layers – compared to reservoir simulation. Int. J. Greenh. Gas. control 10, 389396.
Lie, A., Larsen, D.O., 1991. Monitoring of an underground flow in well 2/4-14 by shallow seismic data. In: Proceedings: the 2/4-14 Experience Transfer Seminar, Stavanger.
Long, D., Laban, C., Streiff, T.D.J., Cameron, T.D.J., Schttenhelm, R.T.E., 1988. The sedimentary record of climatic variation in the southern North Sea. Phil. Trans. Royal Soc. Lond. 318, 523–537.
Løseth, H., Gading, M., Wensaas, L., 2009. Hydrocarbon leakage interpreted on seismic data. Mar. Pet. Geol. 26, 1304–1319.
Mavko, G., Mukerji, T., 1998. Bounds on low-frequency seismic velocities in partially saturated rocks. Geophysics 63, 918924.
Meissner, R., Meixner, E., 1969. Deformation of seismic wavelets by thin layers and layered boundaries. Geophys. Prospect. 17, 1–27.
Michelsen, O., 2001. Late Cenozoic basin development of the eastern North Sea Basin. Bull. Geol. Soc. Den. 43, 9–21.
Nelson, P.H., May 1994. Permeability-porosity relationships. In: Sedimentary Rocks. The Log Analysist. Society of Petrophysicists and Well-Log Analysts.
NPD Fact Pages, 2014. General Information on Exploration Wellbores. Information extracted in July 2014.
Ó Cofaigh, C., 1996. Tunnel valley genesis. Prog. Phys. Geogr. 20, 1–19.
Ottesen, D., Dowdeswell, J.A., Bugge, T., 2014. Morphology, sedimentary infill and depositional environments of the Early Quaternary North Sea basin (56° to 62°). Mar. Pet. Geol. 56, 123–146.
Ottesen, D., Rise, L., Andersen, E.S., Bugge, T., Eidvin, T., 2009. Geological evolution of the Norwegian continental shelf between 61N and 68N during the last 3 million years. Nor. J. Geol. 89, 251–265.
Pekot, L.J., Gersab, G.A., 1987. "Ekofisk": Geology of Norwegian Oil and Gas Fields North Sea. Graham and Trotman, Ltd.
Praeg, D., 2003. Seismic imaging of mid-Pleistocene tunnel-valleys in the North Sea Basinhigh resolution from low frequencies. J. Appl. Geophys. 53, 273–298.
Remen, A., 1991. Flow paths and shallow gas migration. In: Proceedings: the 2/4-14 Experience Transfer Seminar, Stavanger.
Rise, L., Olesen, O., Rokoengen, K., Ottesen, D., Riis, F., 2004. Mid-Pleistocene ice drainage pattern in the Norwegian Channel imaged by 3D seismics. Quat. Sci. Rev. 23, 2323–2335.
Rise, L., Ottesen, D., Berg, K., Lundin, E., 2005. Large-scale development of the mid-Norwegian margin during the last 3 million years. Mar. Pet. Geol. 22, 33–44.
Rutherford, S.T., Williams, R.H., 1989. Amplitude-versus-offset variations in gas sands. Geophysics 54, 680–688.
Sallisbury, R.S.K., Denley, M.R., Douglas, G., 1996. The value of integrating existing 3D seismic into shallow gas studies. In: Proceedings: Offshore Technology Conference (OTC), Jouston Texas.
Sengupta, M., 2000. Integrating Rock Physics and Flow Simulation to Reduce Uncertainties in Seismic Reservoir Monitoring. Ph.D. thesis. Stanford University.
Sernpere, J.E., Hardy, P.B., 1998. Reflection tomography and velocity model building in an area characterized by shallow Gas. In: Proceedings: Offshore Technology Conference (OTC), Jouston Texas.
Sheriff, R., 1985. Aspects of seismic resolution. In: Berg, O.R., Woolverton, D.G. (Eds.), Seismic Stratigraphy: II. An Integrated Approach to Hydrocarbon Exploration, AAPG Memoir, vol. 39, pp. 1–10.
Shuey, R.T., 1985. A simplification of the zöppritz equations. Geophysics 50, 609–614.
Sillis, G.C., Wheeler, S.J., 1992. The significance of gas for offshore operations. Cont. Shelf Res. 12, 1239–1250.
Smith, G.C., Gidlow, P.M., 1987. Weighted stacking for rock property estimation and detection of gas. Geophys. Prospect. 35, 993–1014.
Sørensen, J.C., Gregersen, U., Breiner, M., Michelsen, O., 1997. High-frequency sequence stratigraphy of the Upper Cenozoic deposits in the central and Southeastern North Sea areas. Mar. Pet. Geol. 14, 99–123.
Sørensen, J.C., Michelsen, O., 1995. Upper cenozoic Southeastern North sea Basin. Bull. Geol. Soc. Den. 43, 74–98.
Spjeldnes, N., 1975. Palaeogeography and facies distribution in the Tertiary of Denmark and surrounding areas. Norges Geol. Underskelse (NGU) 316, 289–311.
Stewart, M.A., Lonergan, L., 2011. Seven glacial cycles in the middle-late Pleistocene of northwest Europe: geomorphic evidence from buried tunnel valleys. Geology 39, 283–286.
Stoker, M.S., Long, D., 1984. A relict ice-scoured erosion surface in the Central North Sea. Mar. Geol. 61, 85–93.
Stoker, M.S., Praeg, D., Hjelstuen, B.O., Laberg, J.S., Nielsen, T., Shannon, P.M., 2005. Neogene Stratigraphy and sedimentary and oceanographic development of the NW European Atlantic margin. Mar. Pet. Geol. 22, 977–1005.
Stoker, M.S., Skinner, A.C., Fyfe, J.A., Long, D., 1983. Palaeomagnetic evidence for early Pleistocene in the central and northern North Sea. Nature 304, 332–334.
Stuart, J.Y., Huuse, M., 2012. 3D seismic geomorphology of a large Plio-Pleistocene delta - bright spots and contourites in the Southern North Sea. Mar. Pet. Geol. 38, 85–93.
Syvetski, J.P.M., Andrews, A.B., Milliman, J.D., 1992. Icebergs and the seafloor east Greenland (Kangerlussuaq) Continental margin. Arct. Antarct. Alp. Res. 3, 52–61.
Virieux, J., 1986. P-sv wave propagation in heterogeneous media: velocity-stress finite-difference method. Geophysics 51, 889–901.
Widess, M.B., 1953. How thin is a thin bed? Geophysics 38, 1176–1180.
Woodworth-Lynas, C.M.T., Josenhans, H.W., Barrie, J.V., Lewis, C.F.M., Parrott, D.R., 1991. The physical processes of seabed disturbance during iceberg grounding and scouring. Cont. Shelf Res. 11, 939–961.
Ziegler, P.A., 1988. Evolution of the Arctic-North Atlantic and the Western Tethys. In: AAPG Memoir, vol. 43.
Ziegler, P.A., 1990. Geological Atlas of Western and Central Europe. Geological Society of London.
Zöppritz, K., 1919. Earthquake waves VII VIIb. About reflection and passage of seismic waves on surfaces of discontinuity. Göttinger Nachrichten (Royal Soc. Sci. Göttingen) 1, 66–84.